Ligand-independent IL-6 pathway activation (L-gp130) accelerates the transformation of proliferating human hepatocytes via increased oxidative stress in comparison to ligand-dependent IL-6 pathway activation (Hyper-IL-6)

Dissertation

zur Erlangung des Grades eines Doktors der Medizin
an der Medizinischen Fakultät der Universität Hamburg.

vorgelegt von:

Inés Gil Ibáñez
aus Madrid

Hamburg 2015

Angenommen von der
Medizinischen Fakultät der Universität Hamburg am: 01.09.2015

Veröffentlicht mit Genehmigung der
Medizinischen Fakultät der Universität Hamburg.

Prüfungsausschuss, der Vorsitzende: PD. Dr. med. Henning Wege

Prüfungsausschuss, zweiter Gutachter: Prof. Dr. med. Björn Nashan

"Student: Dr. Einstein, aren't these the same questions as last year's final exam?
Dr. Einstein: Yes, but this year the answers are different."

- Albert Einstein -

Table of Contents

1. Abstract

Presently, a leading hypothesis states that pro-inflammatory signaling pathways, e.g. interleukin 6 (IL-6), and reactive oxygen species (ROS), promote hepatocyte transformation during the course of chronic hepatitis. In order to elucidate the driving oncogenic mechanisms, we activated the IL-6 signal transducer glycoprotein 130 (gp130) in untransformed hTERT-immortalized human fetal hepatocytes (FH-hTERT). We generated FH-hTERT clones with stable expression of a ligand-independent constitutively active gp130 construct (L-gp130). In these FH-hTERT L-gp130 clones, forced gp130 activation alone was not sufficient to induce full malignant growth. Therefore, we challenged the cells with ROS to investigate the role of ROS in the transformation process. To induce oxidative stress, we treated FH-hTERT L-gp130 clones with H_2O_2 after glutathione depletion with DL-buthionine-[S,R]-sulfoximine (BSO). Challenge with H_2O_2/BSO resulted in 2- to 3-fold higher ROS levels and up to 3-fold more DNA-double strand breaks (DSB) in FH-hTERT L-gp130 clones in comparison to parental cells. DSB were determined by immunofluorescent staining for γ-H2AX. Despite higher ROS levels and an increased rate of DSB, FH-hTERT L-gp130 clones survived and even displayed an enhanced proliferation following treatment with oxidative stress, and developed colony growth capabilities in soft agar with a frequency of up to 20 colonies per 5,000 seeded cells (FH-hTERT with/without treatment no colonies, FH-hTERT L-gp130 clones without treatment no colonies). Proliferation was monitored by BrdU incorporation, and anchorage-independent growth was scored in soft agar. We also assessed the expression of DNA-damage and antioxidant response genes by real-time quantitative polymerase chain reaction (qPCR). As possible mechanism, we detected a decreased expression of antioxidant genes, in particular GPX3 and APOE. Finally, to compare ligand-independent with ligand-dependent IL-6 signaling, we activated IL-6 *trans-signaling* with the designer cytokine Hyper-IL-6 and recapitulated the experiments. In contrast to FH-hTERT L-gp130 clones,

FH-hTERT incubated with Hyper-IL-6 did not demonstrate increased ROS levels and, as observed in control cells, proliferation was diminished in response to oxidative stress.

In summary, ligand-independent constitutive activation of gp130 resulted in an enhanced cell cycle turnover despite increased levels of ROS and DSB in contrast to ligand-dependent IL-6 activation by Hyper-IL-6. Increased ROS levels in hepatocytes might be a consequence of an altered gp130-mediated oxidative stress response that leads to the accumulation of unrepaired DSB and finally to transformation.

2. Introduction

2.1. Hepatocellular carcinoma

Hepatocellular carcinoma (HCC) is the most common type of liver cancer, representing 85–90% of primary malignant liver tumors. It is the fifth most frequent tumor and, with more than 750,000 deaths per year, the second most important cause of cancer-related death worldwide [1], [2]. The incidence of HCC increases with age and HCC is more common in men than in women [3]. Incidence rates show huge geographic variation, with South-East Asia and Sub-Saharan Africa being the highest risk areas due to a high prevalence of hepatitis B and C infection. Besides chronic viral hepatitis, alcoholism, hemochromatosis, and Wilson's disease are risk factors leading to chronic liver inflammation with permanent hepatocyte damage and regeneration cycles. At a later time point cirrhosis develops, considered to be the main risk factor for malignant transformation [4], [5].

Whereas the clinical risk factors are well defined, the molecular mechanisms driving HCC development are still poorly understood. Hepatocarcinogenesis is a multistep process in an environment of inflammation, oxidative stress, and hypoxia. As a consequence of continuous damage and regeneration of hepatocytes, genetic alterations frequently occur. Accumulation of critical genetic alterations disturbing the cell homeostasis finally lead to the stepwise development of HCC [6]. HCC also develops in healthy livers, although the percentage is very low in the Western world [7].

Patients with HCC do not have any symptoms, unless they suffer from the symptomatology of the underlying cirrhosis. A small percentage of patients with HCC suffer from unspecific symptoms like pain, weight loss or a palpable mass. Therefore, HCC is most often diagnosed in patients in an already advanced

tumor stage. Only in an early stage, curative treatment is amenable by surgical resection, transplantation, and ablative therapies [8]. For a better management of HCC, more detailed functional molecular studies are needed. A better understanding of the molecular mechanisms underlying hepatocarcinogenesis will most likely lead to novel and improved treatment options, as well as approaches to monitor patients with high risk for liver cancer development.

2.2. Immortalized human fetal hepatocytes as cell culture model

Primary human hepatocytes are considered to be the gold standard to investigate hepatocyte metabolism, cellular regeneration, and hepatotoxicity. However, cultivation of primary hepatocytes leads to cell cycle arrest, de-differentiation, and loss of function [9]. Liver cancer cell lines with permanent proliferation have also been employed, but these cells already exhibit a transformed phenotype with genetic changes in different signaling pathways. For example, the well-characterized cell line HepG2 has already acquired multiple genetic alterations on various chromosomes and cannot be used to study the transformation process [10]. Due to the lack of a suitable human liver cell culture model, the *in vitro* study of the molecular mechanisms driving the stepwise development of HCC is limited. For this reason, our group has previously generated telomerase-immortalized human fetal hepatocytes (FH-hTERT) to investigate human hepatocarcinogenesis [11].

In somatic cells, telomerase is normally suppressed and telomeres progressively shorten with each cell cycle until a critical length is reached and the cells enter senescence [12]. To avoid telomere-related checkpoints, most human cancers acquire permanent telomerase activity [13]. Active telomerase allows the stabilization and even elongation of telomeres and an unlimited cell cycle division [14]. In HCC and many other human cancers, telomerase is activated by the re-expression of the rate-limiting catalytic subunit human telomerase reverse transcriptase (hTERT) [15]. In our FH-hTERT cell culture

model, telomerase activation alone is not sufficient to induce malignant transformation [14], [16]. Therefore, we utilized FH-hTERT cells as hepatocyte-derived cell line with the ability to proliferate beyond senescence while maintaining an untransformed phenotype [11]. FH-hTERT cells have acquired a first mandatory genetic hit (immortalization by telomerase reactivation), but additional molecular changes are required to promote full malignant transformation.

2.3. Pro-inflammatory IL-6 cytokine and liver cancer

HCC is the most prevalent cancer associated with chronic inflammation. It is known that persistent inflammation promotes and exacerbates malignancy and that chronic liver diseases contribute to HCC [17]. In liver inflammation, repetitive hepatocyte damage and proliferation cycles seem to be pivotal in driving the transition from chronic liver injury to dysplasia and HCC. Several cell survival signals are activated and facilitate the accumulation of genetic alterations forcing cancer development [18]. The complex signaling molecules and pathways are interconnected with extensive crosstalk. Identifying and analyzing fundamental inflammatory signaling pathways could lead to the discovery of new predictive biomarkers and targets to treat patients with chronic liver inflammation, thus decreasing their risk of liver cancer development [19].

Major cytokines, chemokines, transcription factors, and proteins are implicated in hepatocarcinogenesis [20]. Among them, interleukin 6 (IL-6) is the major pro-inflammatory cytokine in liver inflammation. Normally, IL-6 participates in immune responses, cell survival, proliferation, and apoptosis during inflammatory processes [21]. On the other hand, it is also known that persistent IL-6 expression together with the activation of the downstream signal transducer and activator of transcription – 3 (STAT3) are implicated in different stages of tumorigenesis. Multiple myeloma, colorectal cancer, gastric carcinoma, and Hodgkin's lymphoma are some of the tumors with elevated IL-6 levels [22].
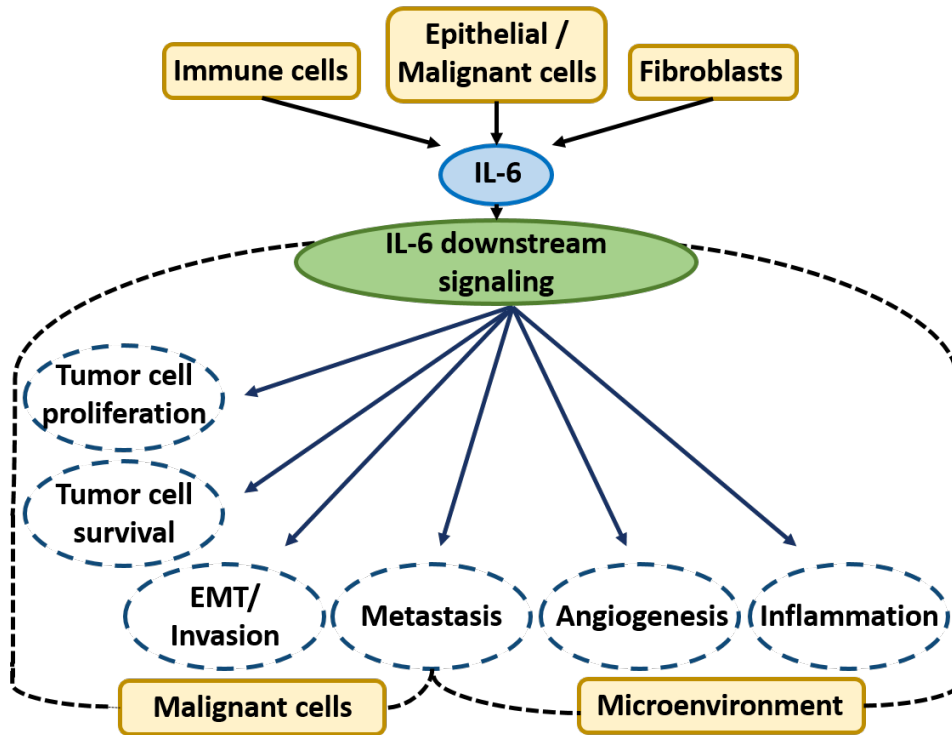
Figure 1. IL-6 signaling in cancer. IL-6, produced by immune cells, epithelial/malignant cells, and fibroblasts, activates several pathways, which in turn induce cell proliferation, survival, epithelial-mesenchymal transition (EMT)/invasion, metastasis, angiogenesis, and inflammation (modified from Taniguchi *et al.* [23]).

Specifically in HCC, elevated IL-6 levels have been reported in patients with chronic liver injury and high risk for HCC [24]. Furthermore, increased serum levels of IL-6 have been directly associated with the stimulation of proliferation, survival, and migration-invasion abilities of HCC cell lines [25]. Moreover, IL-6 is able to promote circulating blood angiogenesis, which is important for self-feeding, growing, and diffusing of malignant cells outside of the liver [26]. Corroborating the relation between HCC and IL-6, a recent clinical study showed a direct correlation between IL-6 levels and the size of the tumor [27].

IL-6 activates several pathways: Janus kinase (JAK)-signal transducer and STAT3 pathway, Src homology 2 (SH2)-containing protein tyrosine phosphatase-2 (SHP-2)-Ras-Raf-MEK-extracellular signal-regulated kinase

(ERK) pathway, and the phosphoinositide 3-kinase (PI3K)-Akt pathway. STAT3 was first identified as an acute-phase protein inductor and an immediate early gene promoter to respond to tissue injury and infection [28]. However, the link between inflammation and cancer is well accepted and STAT3 became also the principal focus of several studies [29], [30], [31]. The activation of STAT3 by IL-6 is a phosphorylation process and is strictly controlled to avoid an aberrant regulation. A deregulation of this phosphorylation results in a constitutive STAT3 activation, which has been detected at a very high frequency (50%-90%) in different human cancers [32], [33], [34]. Specifically in HCC, activated STAT3 is found in 60% of tumors and is more abundant in the aggressive subtypes [35].

In summary, growing evidence indicates that IL-6 activation plays an essential role in inflammation-mediated hepatocarcinogenesis [36]. IL-6 influence has been reported *in vitro* and *in vivo* and, in spite of its still not entirely defined biological function in hepatocarcinogenesis, numerous studies suggest that in addition to controlling liver regeneration, IL-6 also promotes carcinogenesis [37], [38].

2.4 Forced IL-6 signaling in FH-hTERT

There are two possible ways of IL-6 activation: *classic signaling* and *trans-signaling*. In the *classic signaling*, IL-6 binds to a membrane bound interleukin-6 receptor (IL-6R). In *trans-signaling* a soluble form of the interleukin-6 receptor (sIL-6R) is generated, which is able to bind to IL-6. This complex (IL-6/sIL-6R or IL-6/IL-6R) is capable of binding to the gp130 transmembrane receptor (Figure 2) [39]. In both cases, binding of IL-6/IL-6R and IL-6/sIL-6R leads to dimerization of two molecules of gp130 and activation of JAK/STAT3, RAF/MEK/ERK and PI3K-Akt downstream signaling pathways. [40].
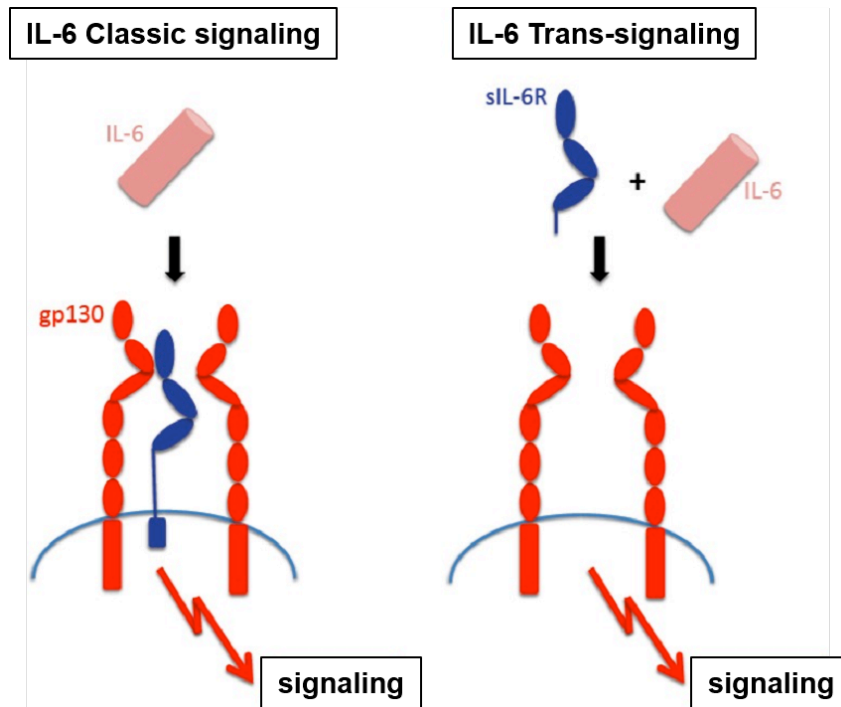
Figure 2. IL-6 pathway activation: *classic signaling* and *trans-signaling*. IL-6 *classic signaling* requires membrane bound IL-6R. In IL-*6 trans-signaling* IL-6 binds to the soluble IL-6R (sIL-6R). In both cases, responses are elicited through the binding to two gp130 molecules that dimerize and subsequently initiate intracellular signaling (modified from Rose-John [41]).

Interestingly, almost all body cells express gp130, whereas IL-6R expression is limited to hepatocytes, neutrophils, monocytes/macrophages, and certain other leukocytes [42]. For IL-6R-deficient cells, *trans-signaling* is the only way to activate IL-6 signaling. This mechanism seems to have a pronounced pro-inflammatory role in the development and progression of different diseases [43], [44]. For example, blockade of IL-6 *trans-signaling* was sufficient to block inflammatory process in autoimmune diseases and inflammation-associated cancer [41].

Previous studies showed that gp130 alone does not show any affinity for IL-6. With a mutated gp130, downstream cascade activation in absence of the ligand is possible [45]. IL-6R or sIL-6R is required to present the ligand IL-6 to gp130 resulting in activation of the intracellular cascades in both signaling pathways [46]. The group of Scheller and Rose-John generated a plasmid coding for a

constitutively active gp130 (L-gp130), responsible for ligand-independent downstream signal transduction (Figure 3) [47].
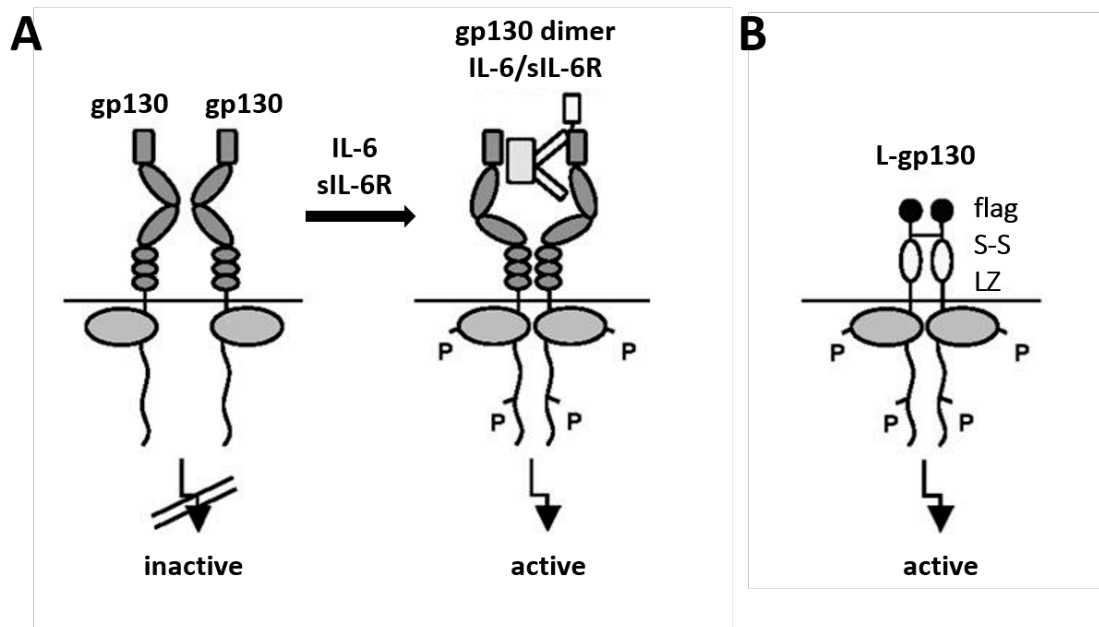
Figure 3. Schematic of the gp130 transmembrane receptor (demonstrated in *trans-signaling*). (A) Gp130 wild-type receptor (gp130). Signal activation is induced after binding of IL-6/sIL-6R. **(B)** Gp130 hybrid receptor L-gp130 constituted with a FLAG-tag (Flag), the signal peptide, and leucine zipper (LZ), and stabilized by an additional disulfide bridge (S-S) (modified from Stuhlmann-Laeisz *et al*. [47]).

To study the role of IL-6 in the transformation of human hepatocytes, IL-6 signaling was activated in untransformed proliferating FH-hTERT cells in a previous doctoral thesis. For this purpose, our group transfected FH-hTERT with L-gp130, kindly provided by Rose-John *et al*., resulting in ligand-independent IL-6 signaling activation. After isolating single-cell clones (FH-hTERT L-gp130 clone 1-3), a possible malignant transformation was investigated by characterizing the phenotype of the clones [48].

First, to monitor IL-6 signaling activation in the clones, phosphorylation of STAT3 and ERK1/2 were investigated and confirmed. To functionally characterize relevant phenotype changes of L-gp130 clones, we monitored

cancer-associated growth properties. FH-hTERT with forced IL-6 signaling activation did not show a completely transformed phenotype: Proliferation was not enhanced in all three clones. Serum-free culture conditions significantly reduced cellular growth in the control cells and clone 3. No significant growth reduction was detected for clone 1 and 2, and therefore, serum dependence was abolished only in theses clones. However, contact inhibition was diminished in all clones. Immediately after stable transfection and selection of clones, no colony formation was observed in soft agar, an *in vitro* marker for malignant growth. Interestingly, in long-term culture the clones developed the ability to generate colonies. In summary, these previous results indicate that forced IL-6 signaling activation does *per se* not induce complete transformation, but predispose the cells to malignant transformation.

2.5. Reactive oxygen species (ROS) in cancer

Reactive oxygen species (ROS) derive from the metabolism of molecular oxygen and have an important role for a proper function of many cellular processes. ROS include superoxide anion radical ($O_2^{\cdot-}$), single oxygen (O_2), hydrogen peroxide (H_2O_2) and hydroxyl radical ($^{\cdot}OH$). In aerobic cell metabolism, ROS are in balance with biochemical antioxidants. Excess ROS, antioxidant depletion, or both, are responsible for the alteration of this balance and the resulting increase in oxidative stress [49]. In the event of cellular stress (e.g. inflammation), it is important that homeostatic parameters counteract oxidative effects and restore redox balance to avoid cellular DNA damage [50]. In hepatocytes, the cytochrome P450 (CYP450) system produces ROS and is involved in removing or detoxifying toxic substances [51]. From diet, exogenous antioxidants, including vitamin C, vitamin E, and carotenoids can be obtained to prevent or reduce oxidative stress and to restore redox balance [52].

Nonetheless, many studies have been conducted to establish that oxidative stress plays a driving role in various clinical conditions, such as atherosclerosis, diabetes, chronic inflammation, viral infection, ischemia-reperfusion injury, and malignant diseases [53], [54], [55], [56]. In the case of cell transformation, inflammatory oxidant stress seems to be by itself insufficient to directly cause cell transformation, but different pro-inflammatory cytokines, growth factors, and adhesion molecules may create a microenvironment that, together with increased levels of ROS, promote neoplastic cell survival and proliferation [57]. For example in HCC, this pro-transformation role of ROS was confirmed in well-established mouse models with spontaneous and chemically induced hepatocarcinogenesis [58]. Moreover, ROS also control the expression of tumor suppressor genes (TP53, Rb, and PTEN) and enhance the expression of proto-oncogenes that support malignant transformation [50], [59].

In the previous study published by Herden [48], FH-hTERT L-gp130 clones were challenged with oxidative stress (treatment with hydrogen peroxide and DL-buthionine-[S,R]-sulfoximine (BSO), a glutathione depleting agent) and showed up to 3-fold higher ROS levels in comparison to treated control cells. To examine DNA-double strand breaks (DSB)-induced cell cycle control mechanisms, p21 expression was measured after ROS treatment, but despite higher ROS levels, p21 expression was similar to the control cells. Moreover, by utilizing a PCR array system, the expression of various genes related to oxidative stress and associated response mechanisms were profiled. Some of the antioxidants genes showed alterations in gene expression in comparison to the control cells.

3. Study aims and significance

Previously generated and characterized FH-hTERT L-gp130 clones showed a pre-malignant phenotype with cancer-associated growth capabilities, such as a less serum-sensitive cell growth and decreased contact inhibition. However, ligand-independent IL-6 activation via L-gp130 was not sufficient to induce a transformed phenotype in our clones. The aim of this study is to investigate oxidative stress as an additional carcinogenic factor and transformation trigger in FH-hTERT cells with gp130-mediated signaling activation (Figure 4).
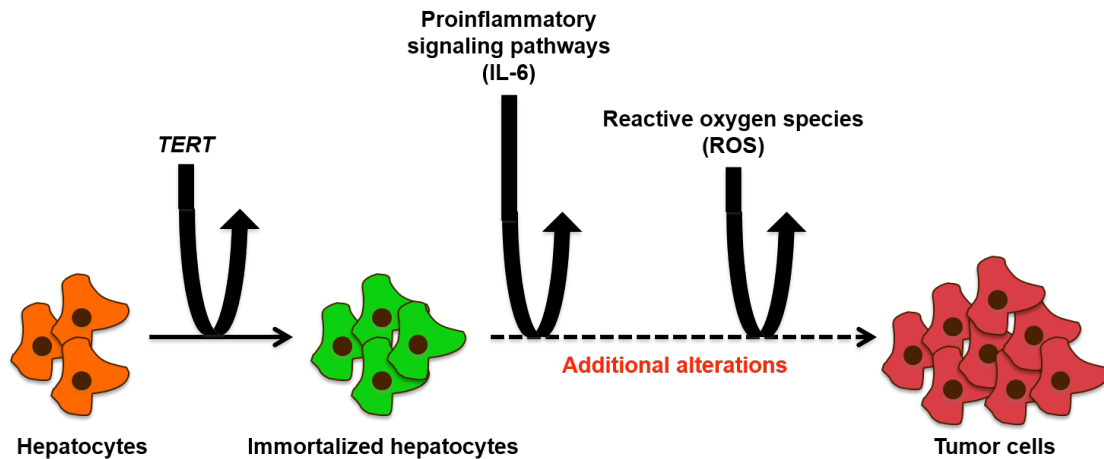
Figure 4. Possible transformation process in hepatocytes. Telomerase activation in hepatocytes promotes unlimited cell cycle division. Pro-inflammatory signaling pathways and oxidative stress constitute possible drivers of the downstream transformation process in immortalized hepatocytes.

To compare ligand-independent signaling via L-gp130 activation with ligand-dependent IL-6 activation, we activated endogenous gp130 in FH-hTERT with the designer cytokine Hyper-IL-6 (Figure 5) and studied the consequences.

Hyper-IL-6

Figure 5. Designer cytokine Hyper-IL-6. IL-6 (pink) is connected by a flexible peptide linker (black) to the sIL-6R (blue) (from Rose-John *et al*. [41]).

A better understanding of the inflammation-associated cellular mechanisms could lead to new diagnostic and therapeutic approaches for patients with chronic hepatitis; and moreover, to novel and highly targeted therapeutic options for patients with HCC.

4. Materials and Methods

4.1. Cell lines

Previously established and characterized telomerase-immortalized human fetal hepatocytes (FH-hTERT) [11] were transfected with the expression plasmid L-gp130 or the backbone vector pcDNA3.1 as control. After selection with antibiotics (Zeocin for L-gp130 or Geneticin for pcDNA3.1, respectively), single cell-clones were generated. In addition to one pcDNA3.1 clone (FH-hTERT pcDNA3.1), three independent L-gp130 clones (FH-hTERT L-gp130 clone 1 to 3) were selected and expanded for further experiments. These clones were generated by our group in a previous doctoral thesis [48]. The described clones have been utilized in the present study. FH-hTERT were used as negative control at population doubling (PD) 36-38. The utilization of FH-hTERT cells was approved by the Ethik-Kommission der Ärztekammer Hamburg (protocol number OB-034/06).

4.2. Cell culture and culture conditions

All cells were cultured in Dulbecco's Modified Eagle Medium (DMEM) including 4.5 g/L glucose (Invitrogen, Karlsruhe, Germany), 10% inactivated fetal bovine serum (FBS; Invitrogen) and gentamicin/amphotericin B (10 µg/mL gentamicin, 0.25 µg/mL amphotericin B; Invitrogen) as antibiotics. For FH-hTERT with and without plasmids, culture medium was supplemented with 5 µg/mL insulin and 2.4 µg/mL hydrocortisone (Sigma-Aldrich, Seelze, Germany). Additionally, for FH-hTERT L-gp130 and FH-hTERT pcDNA3.1, 200 µg/mL Zeocin or Geneticin (Invitrogen) were added to the medium, respectively. All cells were incubated at 37°C in a humidified 5% CO_2 atmosphere (Incubator Heraeus BB 16; Thermo Scientific, Schwerte,

Germany) in tissue culture flasks with a 25 cm² (T25) or 75 cm² (T75) surface (Sarstedt, Nümbrecht, Germany). Cells were splitted depending on the cell confluence (80–100%), generally every 3 days, with a splitting ratio of 1:2 to 1:12 as required for the intended experiment. The cells were washed with phosphate buffered saline (PBS, pH 7.4; Invitrogen) and incubated with 0.25% trypsin-EDTA (Invitrogen) for 2 to 4 minutes at 37°C. Medium was used to stop the digestion and to resuspend the cells. Then, depending on the experiment, cells with the required dilution were seeded. Finally, T25 or T75 flasks were filled up with their appropriate medium and antibiotics, when needed. For precise dilutions, cell counting was done with a Neubauer-counting chamber (Brand, Wertheim, Germany) and a microscope (DM IL; Leica, Wetzlar, Germany). To store the cells, 1×10^6 cells were resuspended in 1 mL freezing medium (80% DMEM, 10% dimethylsulfoxide, 10% FBS) and incubated for 24 to 48 hours at -80°C in a freezing container (Cryo 1° Freezing Container; Nalgene, Rochester, NY, USA). The cells were subsequently transferred to a -160°C liquid nitrogen container (Isothermal V3000-AB Series; Custom BioGenic Systems, Bad Nenndorf, Germany) for long-term storage. A 37°C water bath (GFL, Burgwedel, Germany) was used to thaw the cells. After thawing, cells were resuspended in medium immediately. All cell culture work was carried out under a sterile bench (Heraeus HS 12; Thermo Scientific).

4.3. Incubation with Hyper-IL-6

To compare ligand-dependent IL-6 activation to the IL-6 signaling activation of the L-gp130 clones with stable expression of a constitutively active gp130, we activated the signaling pathway in the parental cell line FH-hTERT by utilizing Hyper-IL-6. The recombinant designer cytokine Hyper-IL-6, kindly provided by Prof. Dr. Stefan Rose-John (Institute of Biochemistry, Christian-Albrechts-Universität zu Kiel), is a complex of human IL-6 connected by a flexible polypeptide chain to the human sIL-6R and is characterized by a better

stability and an increased activity [60]. For Hyper-IL-6 incubation, a 10 ng/mL and a 50 ng/mL working concentration were used. Depending on the experiment, the incubation with Hyper-IL-6 varied from 10 minutes to 12 hours. For the monitoring of cell proliferation, Hyper-IL-6 was added to the medium after the first cell count and Hyper-IL-6-medium was changed on the fourth day.

4.4. Detection of IL-6 signaling activation

After Hyper-IL-6 incubation, we performed Western blot analysis to monitor IL-6 signaling pathway activation. FH-hTERT cells were incubated with Hyper-IL-6 as described above for 10 minutes. For every sample, cells were seeded in T25 and treated when 70-80% confluent. First, protein lysates were extracted and quantified. Following separation of the proteins by SDS-PAGE, proteins were transferred to a nitrocellulose membrane and stained with antibodies specific to the downstream signaling targets p-STAT3 and p-ERK. These two proteins are activated by phosphorylation in response to IL-6 signaling activation [61], [62].

Protein extraction
Treated cells were harvested and protein extracts were prepared by resuspending the cell pellets in 100 µL ice-cold RIPA buffer (PBS, 1% Igepal CA-630, 0.5% sodium deoxycholate, 0.1% SDS) containing protease inhibitors (1 tablet for 10 mL RIPA buffer; Roche Diagnostics, Rotkreuz, Switzerland). Lysates were then passed several times through a 21 gauge syringe to shear genomic DNA. After incubation on ice for 45 minutes, lysates were sonicated (Cycle 4 x 10%) (Sonopuls HD 2070; Bandelin, Berlin, Germany) and centrifuged at 10,000 x g for 15 minutes at 4°C (Eppendorf Centrifuge 5810 R; Eppendorf AG, Hamburg, Germany). Finally, supernatants containing proteins were transferred to tubes and stored at -80°C.

Protein quantification

Protein concentration was quantified with BCA Protein Assay Kit (Pierce Biotechnology, Waltham, MA, USA) according to manufacturer instructions. The method is based on the reduction of Cu^{+2} to Cu^{+1} by protein. Cu^{+1} are quantified by colorimetric detection using bicinchoninic acid (BCA) and the absorbance is measured at 540 nm with a 96-well plate reader (Ultra Microplate Reader EL 808; Bio-Tek Instruments, Winooski, VT, USA). The kit provides a protein standard with defined concentrations of bovine serum albumin (BSA) and protein concentrations are determined based on the standard curve to ensure equivalent amounts of protein loading [63]. 40 µg protein of each sample were diluted in total 30 µl sterile water with 1 x Lammli (250 mM, 10% SDS, 0.5% bromphenolblue, 50% glycerol, 0.5 M DTT in 50 ml distilled water). Finally, the samples were incubated for 5 minutes at 95°C.

Western blot analysis

Proteins were separated according to their molecular weight by sodium dodecyl sulfate polyacrylamide gel electrophoresis (SDS-PAGE). All buffers and the polyacrylamide gel contain sodium dodecyl sulphate (SDS; Sigma-Aldrich). This reagent is an anionic detergent, which covers the proteins with a negative charge. Because of the negative charge, the proteins move by 180 V through the polyacrylamide gel (12%), which is incubated in electrophoresis buffer (15 g Tris base, 72 g glycine, 5 g SDS in 500 mL distilled water), to the positively charged electrode during 1 hour. Proteins are separated according to their molecular size. Then, proteins were transferred to a 0.45 µm nitrocellulose membrane (BIO-RAD, München, Germany) by blotting for 1 hour with transfer buffer (48 mM Tris base, 39 mM glycine, SDS, 20% methanol in distilled water) at 300 mA [64]. Subsequently, the membrane was blocked for 1 hour with 5% non-fat dry milk in 1 x TBST (10 mM Tris-HCl pH 7.6, 150 mM NaCl, 0.05% Tween-20 in distilled water) and incubated with primary antibody solution detecting p-STAT3 or p-ERK, respectively (1:1000 diluted in blocking buffer) at 4°C overnight (Cell Signaling Technology, Waltham, MA, USA). Incubation with species-specific secondary antibody

solution (1:2000 diluted in blocking buffer; Cell Signaling Technology) conjugated with horseradish peroxidase was performed for 1 hour at room temperature. Detection was achieved with the SuperSignal West Dura Extended Duration Substrate (Thermo Scientific). Finally, after stripping the membrane, actin was also visualized as a loading control (Cell Signaling Technology).

4.5. Flow cytometric analysis

Fluorescence-activated cell sorting (FACS) is a method, which allows counting and characterization of single cells based on their physical and molecular characteristics. In this study, fluorescence-based flow cytometry with the flow cytometer FACSCanto (BD Biosciences, Franklin Lakes, NJ, USA) was utilized to measure the levels of ROS via the fluorescent substrate Carboxy-DCF and proliferation by quantification of bromodeoxyuridine (BrdU) incorporation. The incorporated BrdU is stained with specific anti-BrdU fluorescent antibodies. The levels of cell-associated BrdU are then measured by flow cytometry. Furthermore, the diffraction and the scattering of light give information about the cell size and structure, and cell debris and doublets can be excluded [65]. The analysis was performed with the Software FACSDiva5 (BD Biosciences).

4.6. Induction of oxidative stress

In the context of chronic liver injury, oncogenic events are driven by genotoxic ROS. To identify the critical molecular mechanisms, we induced oxidative stress in our cell clones. We treated the cells with 400 µM H_2O_2 (Sigma-Aldrich) and 5 µM BSO (Sigma-Aldrich). BSO is a glutathione depleting agent and therefore inhibits the degradation of ROS [66], [67].

4.7. Detection of ROS

To measure oxidative stress, we used the oxidative stress indicator 5-(6)-carboxy-2′,7′-dichlorodihydrofluorescein diacetate (Carboxy-H_2DCFDA, 10 mM stock solution in DMSO; Invitrogen). This non-fluorescent molecule is converted to a green-fluorescent form (Carboxy-DFC) when acetate groups are removed by intracellular esterases and oxidation by ROS occurs [68]. The final product Carboxy-DCF can be quantified by FACS analysis. In our study, 0.25×10^6 cells were seeded in T25 and cultured until 80-90% confluent. After 6 hours of Hyper-IL-6 incubation, the cells were washed with warm Hank's Balanced Salt Solution (HBSS; Invitrogen) and incubated with 25 μM Carboxy-H_2DCFDA diluted in HBSS for 30 minutes at 37°C in the dark. Once washed with HBSS (37°C), oxidative stress induction was performed as described above. After 1 hour treatment, the cells were washed with PBS and removed with Trypsin-EDTA. Cells were transferred through a cell strainer (70 μm). Following centrifugation (4°C, 5 minutes, 500 x g) cell pellets were washed with PBS and resuspended in 500 μL PBS and directly analyzed by FACS.

4.8. Detection of DNA-double strand breaks

ROS cause cellular damage and genomic instability by inducing, in particular, DSB [69]. In the case of DNA damage, the histone H2AX is phosphorylated and then called γ-H2AX. Because of this modification, the DNA is less condensed, DNA repair can start, and the repair machinery is recruited. To detect the amount of DSB after H_2O_2/BSO treatment, we visualized γ-H2AX foci by fluorescent staining according to Koch *et al.* [70]. Briefly, cells with 70-80% confluence grown on culture slides (BD Bioscience) were treated with H_2O_2/BSO as described before. After 12 hours, the clones were fixed in 2% formaldehyde for 15 minutes, washed four times in PBS for 5 minutes, permeabilized on ice for 5 minutes with 0.2% Triton X-100 in 1% BSA/PBS,

washed in 1% BSA/PBS and blocked with 3% BSA/PBS for 1 hour at room temperature. After incubation with anti-γH2AX antibody (1:100 in 0.5% Tween 20 in 1% BSA/PBS, #05-636; Millipore, Billerica, MA, USA) for 1 hour, slides were washed three times for 10 minutes in 0.5% Tween 20 in 1% BSA/PBS and incubated with Alexa Fluor 594 goat anti-mouse IgG (1:600 in 0.5% Tween 20 in 1% BSA/PBS, #A11005; Molecular Probes, Darmstadt, Germany) for 1 hour at room temperature. For an equitable distribution of the antibodies, the chambers were covered with plastic coverslips (Nunc, Roskilde, Denmark) during the incubation with the antibodies. Finally, cells were washed four times for 10 minutes in 0.5% Tween 20 in PBS, counterstained with Hoechst (1:20,000; Invitrogen) and mounted. Fluorescence images were captured by using the HS All-in-one Fluorescence Microscope BZ-9000E (Keyence, Neu-Isenburg, Germany). For quantitative analysis, foci were counted using a 40-fold magnification. One hundred cells per treatment per slide and experiment were evaluated blindly. Rad51 foci were detected with anti-Rad51 antibody (1:1000 in 0.5% Tween 20 in 1% BSA/PBS, #ab213-100; Abcam, Cambridge, UK) and Alexa Fluor 594 goat anti-mouse IgG. As positive control, FH-hTERT cells (60–70% confluence) were exposed to γ-radiation (6 Gy), cultured for 24 hours, and fixed and stained as described before.

4.9. Cell proliferation

Cell counting

To monitor cell proliferation, we performed cell counting over a period of 7 days. 20,000 cells per well were seeded in 24-well plates (Nunclon Surface; Nunc) and every other day, 4 wells were counted per cell clone. The mean cell number was calculated and the average increase in cell number was obtained by comparing the reading to the mean cell number obtained 24 hours after seeding. For Hyper-IL-6-incubated FH-hTERT, Hyper-IL-6 was added to the medium after the first count.

BrdU-assay

To detect the effect of oxidative stress on DNA synthesis, proliferation was determined with APS BrdU Flow Kit (BD Bioscience). BrdU is an analogue of thymidine and incorporated into newly synthesized DNA of replicating cells during the S-phase of the cell cycle. The S-phase fraction can then be determined using fluorescent antibodies specific for BrdU. Additionally, 7-aminoactinomycin D (7-AAD) was utilized to stain the full amount of DNA. In our study, 0.35×10^6 cells were seeded per T25 and cultured until 70-80% confluence. Following the indicated incubation (Hyper-IL-6 for 1 hour and/or H_2O_2/BSO for 12 hours), cells were incubated for 45 minutes at 37°C with BrdU at a final concentration of 10 µM in cell culture medium. The following fixation and staining procedure was performed according to the manufacturer's protocol. Finally, S-phase fractions were determined by FACS analysis.

4.10. Colony assay

To determine anchorage independent growth, one of the characteristics of tumor cells, soft agar colony assays were performed. Per 60-mm tissue culture dish, 5,000, 10,000, or 20,000 cells were diluted in 0.33% agar and overlaid onto 0.5% base agar. After 3 to 4 weeks, colony formation was observed and quantified with a phase-contrast microscope. HepG2 cells were used as positive control (800 seeded cells per dish). To induce oxidative stress, cells were incubated with H_2O_2/BSO 12 hours before seeding.

4.11. Tumor formation in nude mice

To investigate malignant transformation *in vivo*, L-gp130 clones were transplanted in 4- to 10-week-old NMRI athymic nude mice. All animal experiments were approved by the local review board (protocol number 6/12)

and all animals received human care. Per cell clone, 3 mice were transplanted by inoculating 2 x 10^6 cells in 100 µL culture medium with 2% serum and mixed with 100 µL Matrigel (Sigma-Aldrich) subcutaneously into the dorsal flanks of both sides. We observed tumour formation for a minimum of 12 months and animals were monitored once per week until they developed tumors. At that time, tumor growth was measured twice per week using a calliper. As negative control, FH-hTERT pcDNA3.1. cells were transplanted.

4.12. Changes in the expression of antioxidative defence genes

RNA isolation

To quantify gene expression of genes involved in oxidative stress response, total RNA was extracted with the NucleoSpin RNA II Kit (Macherey-Nagel, Düren, Germany). With the included rDNase solution, the DNA was removed and pure RNA was eluted with RNase-free H_2O. RNA concentration was determined by measuring the absorption at 260 and 280 nm with a spectrophotometer (Nanodrop, Wilmington, DE, USA).

cDNA synthesis

After RNA extraction, cDNA synthesis was performed with the Transcriptor First Strand cDNA Synthesis Kit (Roche). Per sample, 1 µg total RNA was used and transcribed with the thermocycler GeneAmp PCR System 9700 (Applied Biosystems, Waltham, MA, USA). Final cDNA concentration was 50 ng/µL.

Quantitative real-time PCR

For quantitative real-time PCR (qPCR), we employed validated primer sets from Qiagen (QuantiTect Primer Assay, Venlo, Netherlands) for NAD(P)H dehydrogenase quinone 1 (NQO1), glutathione peroxidase 3 (GPX3), cytoglobin (CYGB), superoxide dismutase 3 (SOD3), apolipoprotein E (APOE), 24-dehydrocholesterol reductase (DHCR24), selenoprotein P 1

(SEPP1), in combination with QuantiTect SYBR Green PCR Fast Master Mix (Qiagen). As internal control, four different reference genes were combined as a basket housekeeper and mean cycle number at threshold (Ct) values were used for comparative quantification: glycernaldehyde-3-phosphate-dehydrogenase (GAPDH), ß-2-microglobulin (B2M), TATA-box binding protein (TBP), ribosomal protein L13a (RPL13A). Expression levels were determined by an efficiency-corrected model and by using FH-hTERT as calibrator and control with a relative expression of 1 ($E^{\Delta Ct \text{ (gene of interest)}}/E^{\Delta Ct \text{ (basket housekeeper)}}$) [71]. For each sample, 5 µl 2x QuantiFast SYBR Green PCR Fast Master Mix, 1 µl 10x QuantiTect Primer Assays (diluted with Tris and EDTA buffer [TE]), 3 µl distilled water and 1 µl cDNA (25 ng/µL) were combined and PCR (95˚C for 10 minutes, 40 cycles with denaturation by 95˚C for 10 seconds and annealing/extension by 60˚C for 30 seconds) was done in a 384-well plate on the Real-Time PCR System ViiA7 (Applied Biosystems).

4.13. Statistical analysis

All experiments were performed at least in triplicates and with two to three repetitions. Data are presented as mean ± standard deviation (SD). The unpaired Student´s t-test was used for statistical analysis and P values less than 0.05 were considered statistically significant.

5. Results

5.1. Transformation of FH-hTERT L-gp130 clones

Previously, our group transfected FH-hTERT cells with L-gp130 resulting in ligand-independent IL-6 signaling pathway activation. After isolating single-cell clones (FH-hTERT L-gp130), clone 1-3 were characterized. Robust IL-6 signaling activation in these clones was verified by detecting phosphorylation of STAT-3 and ERK1/2. Next, proliferation, serum dependence, colony formation, and contact inhibition were investigated. FH-hTERT L-gp130 clones did not show a completely transformed phenotype, but the results indicate a predisposition to malignant transformation [48].

5.1.1. Tumor formation in athymic nude mice

To confirm the potential for malignant transformation *in vivo*, the clones were transplanted into athymic nude mice and tumor formation was observed. FH-hTERT pcDNA3.1. cells were used as control (Table 1).

Table 1. Tumor formation

Clone	Transplantation sites (n)	Number of tumors	Frequency (%)	Latency (w)
FH-hTERT pcDNA3.1.	6	0	0	NA
FH-hTERT L-gp130 clone 1	6	4	66.7	8.5 ± 0.7
FH-hTERT L-gp130 clone 2	6	0	0	NA
FH-hTERT L-gp130 clone 3	6	2	33.3	10.3 ± 0

NA = not applicable; Mean ± SD.

Within a latency period of 8.5 ± 0.7 and 10.3 ± 0 weeks respectively, FH-hTERT Lgp130 clone 1 and FH-hTERT L-gp130 clone 3 showed tumor formation in contrast to control cells (FH-hTERT pcDNA3.1.) and FH-hTERT L-gp130 clone 2. In the case of FH-hTERT L-gp130 clone 1, tumor growth was observed in 66.7% of transplantation sites. FH-hTERT L-gp130 clone 3 showed tumor formation in 33.3% of transplantation sites.

5.1.2. Colony formation under the influence of oxidative stress

Immediately after activation of IL-6 signaling, FH-hTERT L-gp130 clones were not able to form colonies in soft agar. However, in long-term expansion culture, all three clones developed the ability to generate colonies. To investigate if ROS accelerate the transformation process occurring in long-term culture, we challenged the clones with oxidative stress. After treatment with H_2O_2/BSO, FH-hTERT L-gp130 clones were seeded in soft agar and colony formation was monitored after 4 weeks (Figure 6).
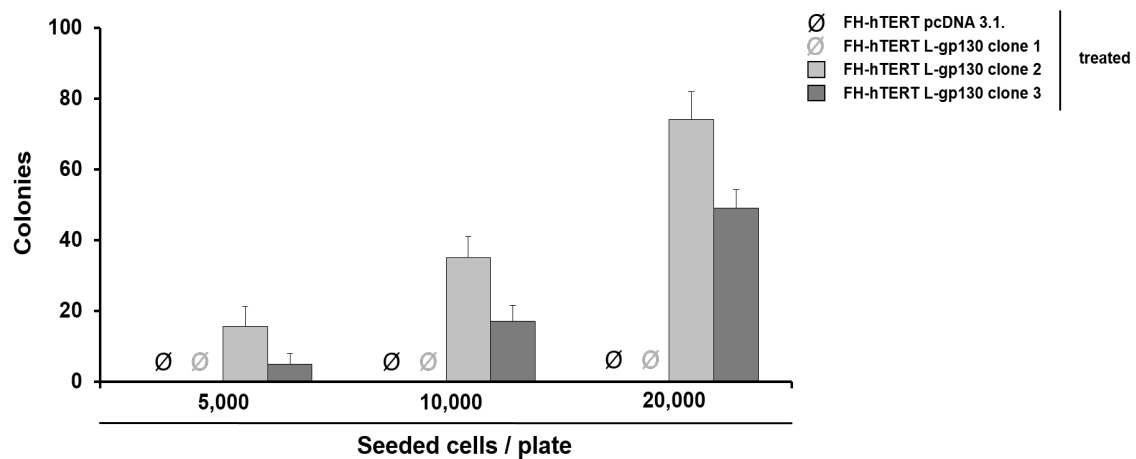

Figure 6. Colony formation induced by oxidative stress. Number of colonies per 5,000, 10,000, and 20,000 seeded cells on culture dishes after 4 weeks. FH-hTERT pcDNA 3.1. seeded as control.

In treated FH-hTERT and FH-hTERT L-gp130 clone 1, no colony formation was observed after 4 weeks. However, treated FH-hTERT L-gp130 clone 2 and 3 repeatedly showed colony formation. Thus, challenge with oxidative stress accelerated the transformation process and colony formation was induced by H_2O_2/BSO treatment.

5.2. Analysis of mechanisms leading to transformation

5.2.1. Detection of DSB

Challenge with H_2O_2/BSO led to higher ROS levels in L-gp130 clones. To test if these higher ROS levels result in more DNA damage, DSB were quantified via γ-H2AX fluorescence staining (Figure 7).
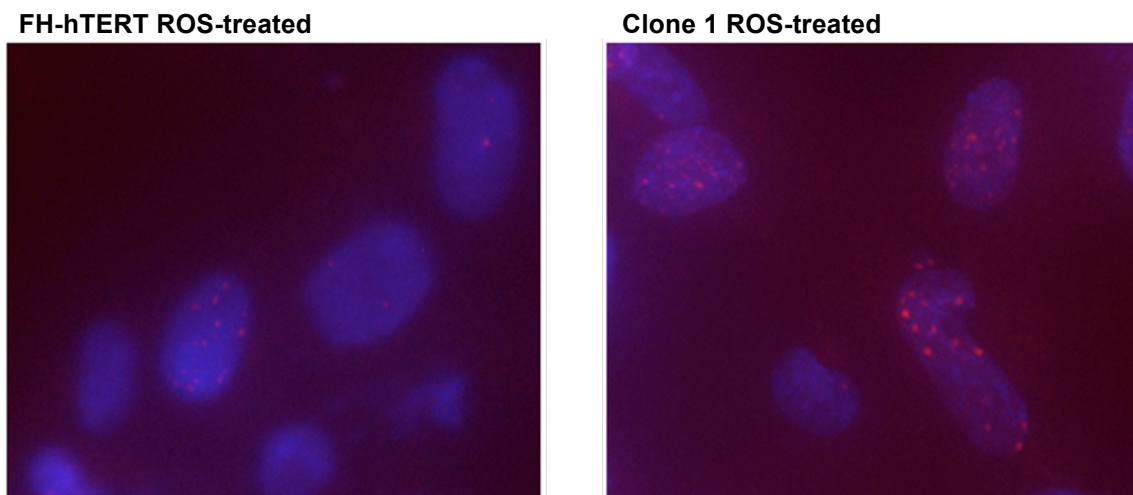
FH-hTERT ROS-treated

Clone 1 ROS-treated

Figure 7. Visualization of DNA-double strand breaks. γ-H2AX foci were visualized by fluorescent staining (red points). ROS-treated FH-hTERT cells showed small and hardly visible foci (left), whereas ROS-treated FH-hTERT L-gp130 clone 1 cells, for example, showed big and numerous foci (right). Cell nuclei were counterstained with DAPI (blue).

H_2O_2/BSO treatment induced higher numbers of γ-H2AX foci in all three clones, indicating extensively more DSB. In contrast, in FH-hTERT cells the number of γ-H2AX foci was lower than in the clones. The difference between ROS-treated

FH-hTERT and ROS-treated FH-hTERT L-gp130 clone 2 and 3 was statistically significant (Figure 8).
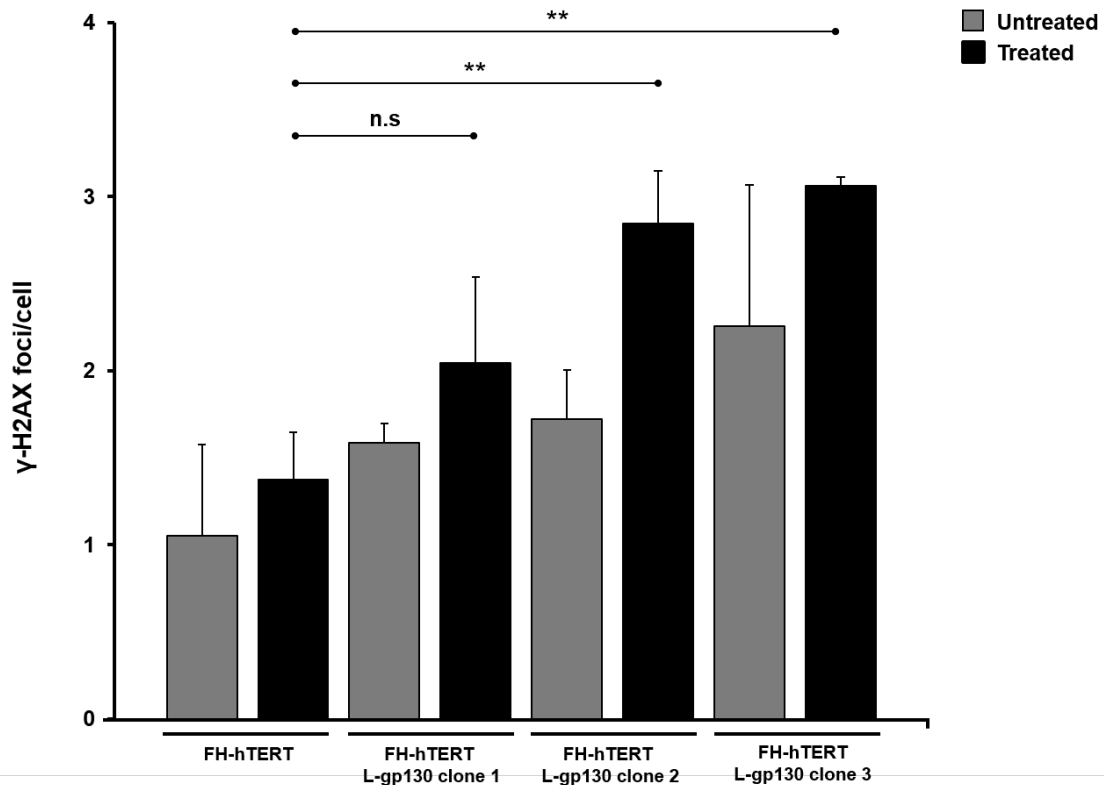

Figure 8. Quantitative analysis of γ-H2AX foci. Quantification of γ-H2AX foci formation is expressed as average number of foci per cell with SD as error bars. *P*-values are as indicated, *P*<0.01 (**).

5.2.2. Proliferation rate

As summarized before, H_2O_2/BSO-treated clones showed higher ROS levels und more DSB than treated control cells. However, L-gp130 clones did not show the expected higher growth arrest rate, as indicated by a diminished p21 upregulation. To confirm these results, we determined S-phase fractions of ROS-treated and untreated cells by BrdU-incorporation and FACS quantification. Representative dot plots are shown in Figure 9.
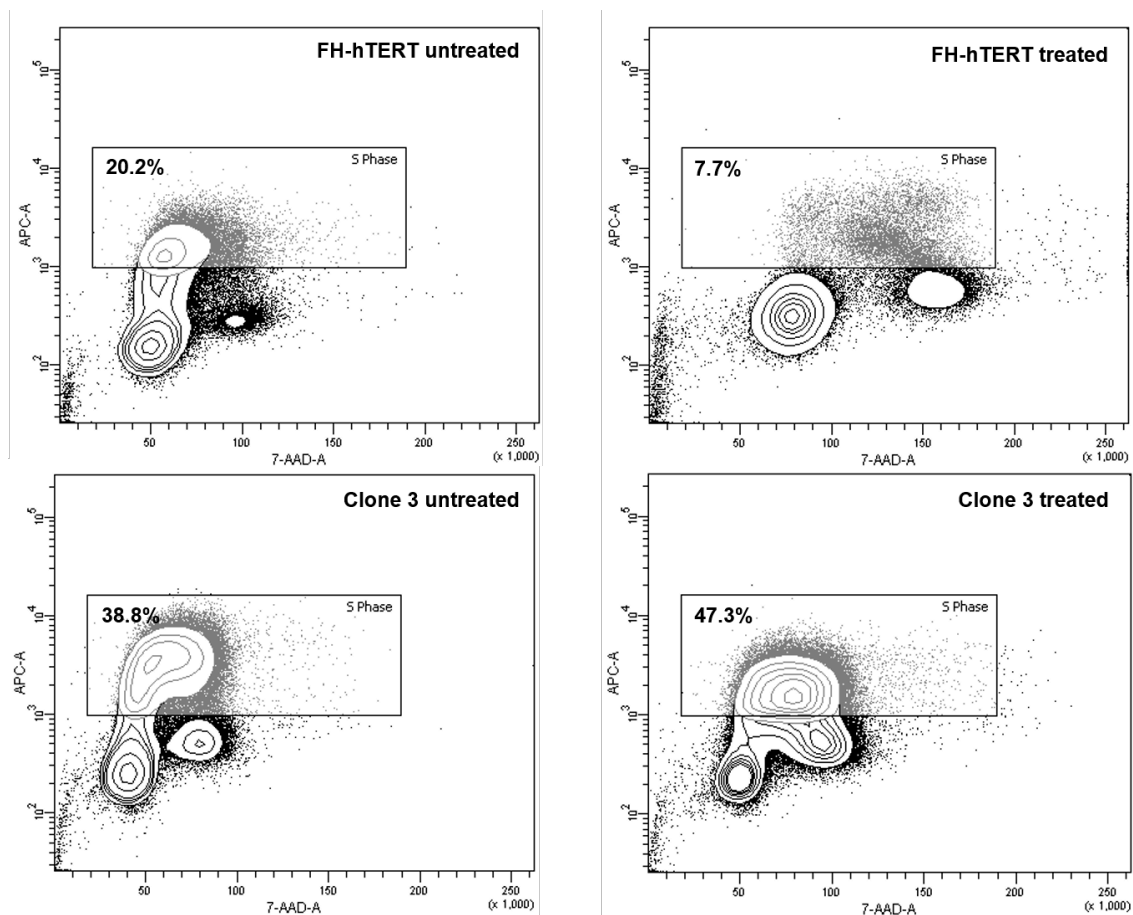
Figure 9. Flow cytometric measurement of total DNA and incorporated BrdU. Representative BrdU APC-A *versus* DNA 7-AAD-A plots (FSC-A *versus* SSC-A gated cell population) showing G0/G1, S and G2/M fractions, are shown for control cells and clone 3 with and without ROS treatment.

S-phase fractions of untreated FH-hTERT L-gp130 clones were between 30-40%. Following H_2O_2/BSO treatment, FH-hTERT displayed a reduction in the S-phase fraction by 73.6% ± 2.3%, indicating cell cycle arrest induced by oxidative stress. In contrast, the L-gp130 clones did not show a reduction in S-phase fraction and even an increased BrdU incorporation. In FH-hTERT L-gp130 clone 1-3 an increase of 34.6% ± 2.3%, 40.1% ± 11.2%, and 27.4% ± 21.9% was detected (Figure 10).
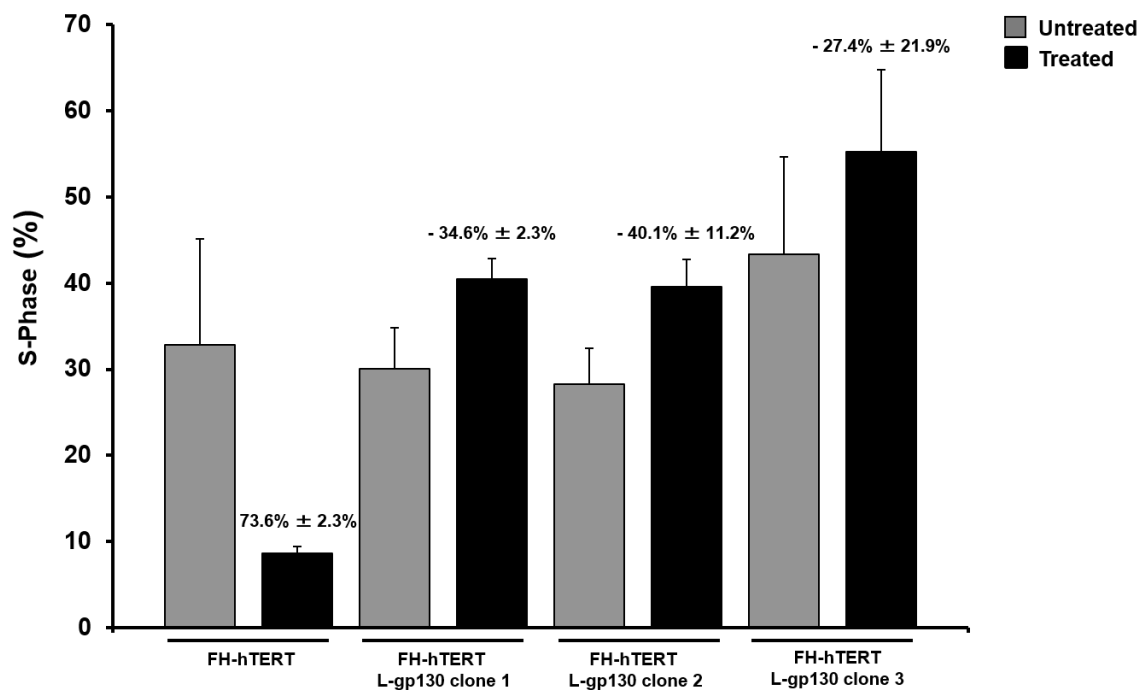
Figure 10. S-phase analysis under oxidative stress determined by BrdU incorporation assay. The bars represent the average S-phase fractions ± SD (error bars) of untreated (■) and treated (■) cells. The data above black bars represent change in S-phase fraction of treated cells in comparison to untreated (negative S-phase reduction indicates an increase).

5.2.3. Changes in antioxidative defense

In order to understand the mechanism leading to higher ROS levels in our clones following H_2O_2/BSO treatment, we previously profiled the expression of various genes related to oxidative stress and response mechanisms employing PCR array technology. The assay revealed altered expression levels for GPX3, CYGB, SOD3, APOE, DHCR24, and SEPP1 in all three L-gp130 clones. In this study, we monitored these genes in our L-gp130 clones with and without additional ROS challenge by qPCR. Additionally, we measured NQO1 expression. NQO1 is one of the target genes of NRF2, which initiates an antioxidative transcription program (Figure 11 and 12).
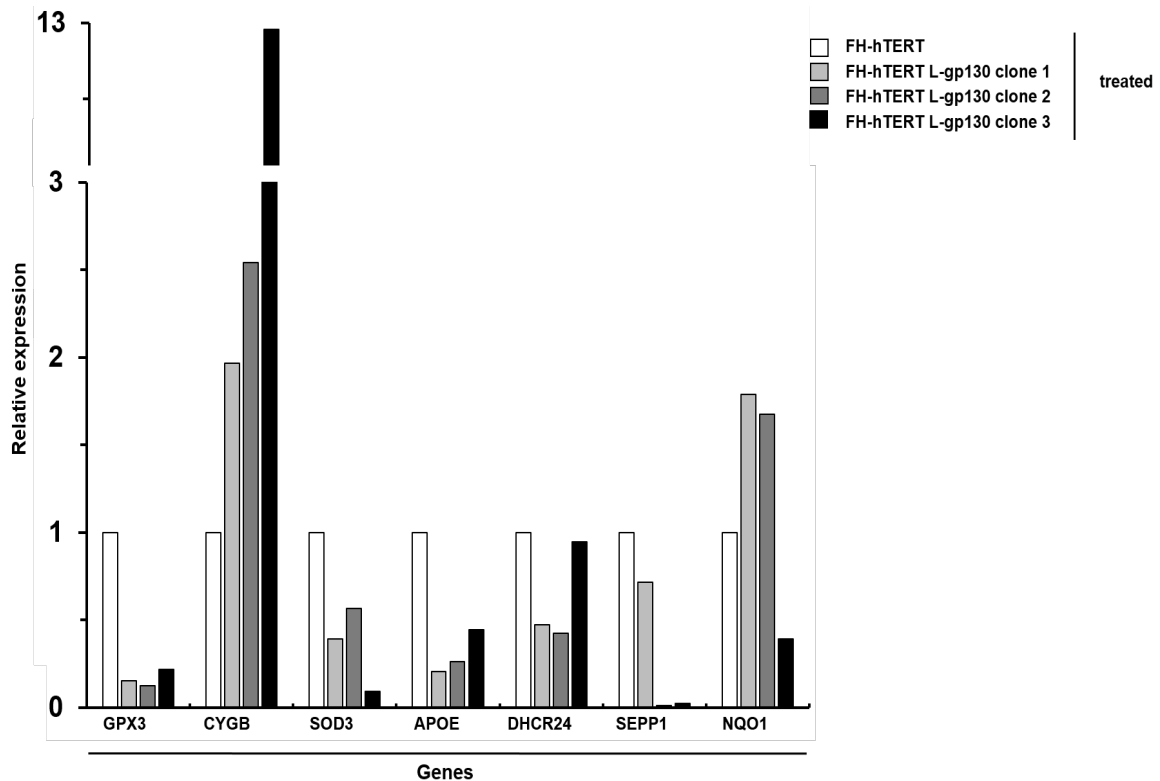
Figure 11. qPCR of genes involved in oxidative stress defense 7 hours post ROS exposure. Relative expression of GPX3, CYGB, SOD3, APOE, DHCR24, SEPP1, and NQO1 in L-gp130 clones in comparison to the control cells FH-hTERT (expression level = 1).

After 7 hours of treatment with H_2O_2/BSO, all three clones showed lower expression levels for GPX3 (clone 1: 0.152, clone 2: 0.124, clone 3: 0.216). For CYGB, expression was much higher in all three clones than in the control (clone 1: 1.967, clone 2: 2.543, clone 3: 12.956). The gene expression of SOD3 and APOE was lower in all clones than in untreated control cells (relative expression of SOD3 in clone 1: 0.393, clone 2: 0.567, clone 3: 0.091; relative expression of APOE in clone 1: 0.206, clone 2: 0.263, clone 3: 0.443).

Under normal conditions, the antioxidative effect of DHCR24 is observed when it is down-regulated. In our experiment, this effect was only seen in clone 1 and 2. FH-hTERT L-gp130 clone 3 exhibited similar DHCR24 expression levels in comparison to FH-hTERT cells (clone 1: 0.472, clone 2: 0.423, clone 3: 0.945). SEPP1 expression was clearly reduced in all treated clones, but not in FH-

hTERT L-gp130 clone 1 (clone 1: 0.715, clone 2: 0.011, clone 3: 0.022). Lastly, in two clones NQO1 expression was higher than in treated FH-hTERT. Only, treated FH-hTERT L-gp130 clone 3 showed lower expression levels compared to treated control cells (clone 1: 1.788, clone 2: 1.677, clone 3: 0.392).
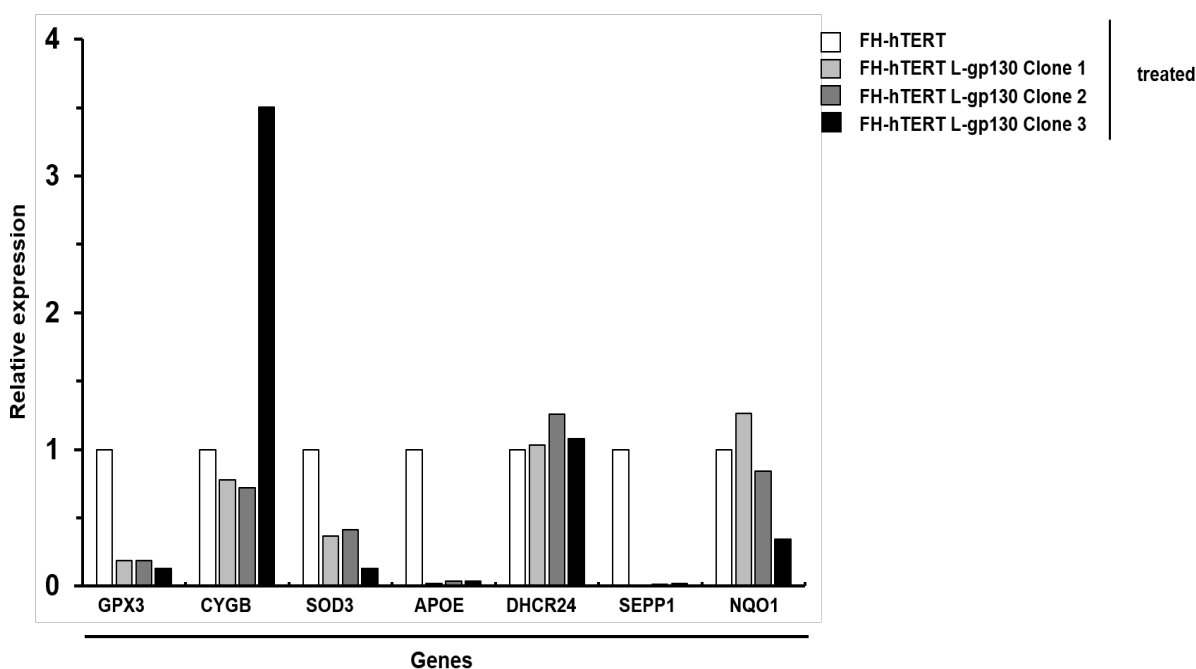
Figure 12. qPCR analysis of genes involved in oxidative stress defense 12 hours post ROS exposure. Relative expression of GPX3, CYGB, SOD3, APOE, DHCR24, SEPP1, and NQO1 in L-gp130 clones in comparison with the control cells FH-hTERT (expression level = 1).

After 12 hours treatment with H_2O_2/BSO, all three clones showed lower expressions levels of GPX3, APOE, and SEPP1 in comparison to treated FH-hTERT (relative expression of GPX3 in clone 1: 0.187, clone 2: 0.189, clone 3: 0.127; relative expression of APOE in clone 1: 0.020, clone 2: 0.038, clone 3: 0.037; relative expression of SEPP1 in clone 1: 0.005, clone 2: 0.011, clone 3: 0.20). For CYGB, expression levels in clone 1 and 2 were slightly reduced in comparison to treated control cells. However, CYGB expression of clone 3 was up to 3-fold higher than in treated FH-hTERT cells (clone 1: 0.799, clone 2: 0.720, clone 3: 3.502). All three clones presented lower gene expression of

SOD3 than treated control cells (clone 1: 0.367, clone 2: 0.413, clone 3: 0.129). DHCR24 expression was similar in all treated clones (clone 1: 1.030, clone 2: 1.260, clone 3: 1.077). Finally, in comparison to treated control cells, only FH-hTERT L-gp130 clone 1 showed higher NQO1 expression (clone 1: 1.264, clone 2: 0.840, clone 3: 0.342).

5.3. Ligand-dependent IL-6 activation by Hyper-IL-6

Hyper-IL-6 is a designer protein characterized by a better stability and higher affinity to gp130. To evaluate the impact of genetic activation of IL-6 signaling in our cell culture model in comparison to ligand activation, we recapitulated our experiments and performed ROS challenge in FH-hTERT incubated with Hyper-IL-6.

5.3.1. IL-6 signaling activation

To confirm the activation of IL-6 signaling pathway in FH-hTERT after Hyper-IL-6 incubation, p-STAT3 was determined following incubation with 10, 50 and 100 ng/ml Hyper-IL-6. β-Actin served as control (Figure 13).
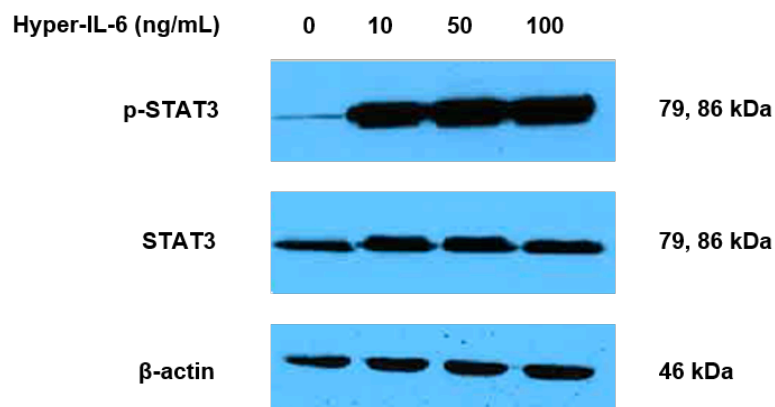
Figure 13. IL-6 signaling activation mediated by Hyper-IL-6. Phosphorylation of STAT3 in FH-hTERT incubated with different Hyper-IL-6 concentrations was determined by immunoblotting. 40 µg protein per sample was loaded. β-Actin was visualized as loading control.

After 10 minutes, a robust phosphorylation of STAT3 was detected indicating IL-6 signaling pathway activation. A minimal pathway activation was observed in FH-hTERT without incubation by Hyper-IL-6. For further experiments, concentrations of 10 and 50 ng/ml were used.

5.3.2. Proliferation analysis

To compare proliferation of FH-hTERT L-gp130 clone 1-3 and Fh-hTERT incubated with Hyper-IL-6, proliferation was monitored for 7 days by cell counting every other day (Figure 14 and 15).

Figure 14. Cell proliferation of FH-hTERT L-gp130 clone 1-3. Each time point represents the mean of 4 independent cell counts. *P*-values are as indicated, *P*<0.05 (*).

Contrary to our assumption, L-gp130 clone 1 and 2 did not show an accelerated cellular growth in comparison to the control cells. Only, clone 3 displayed an increased proliferation.
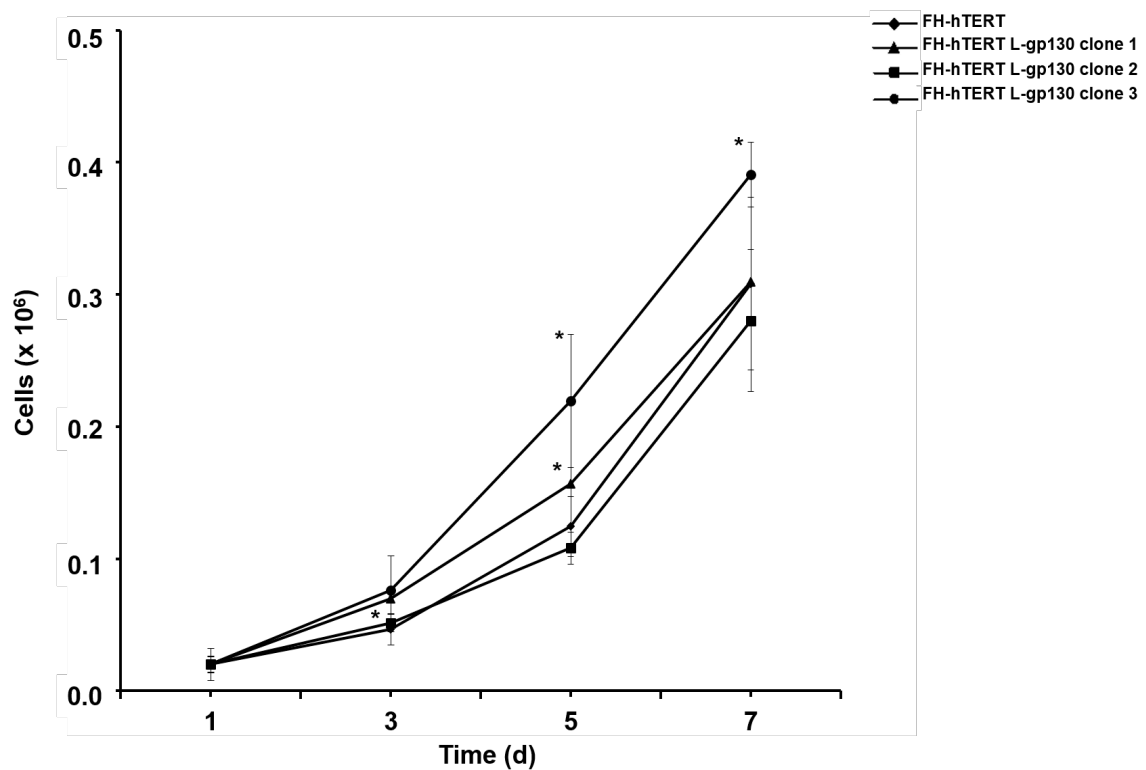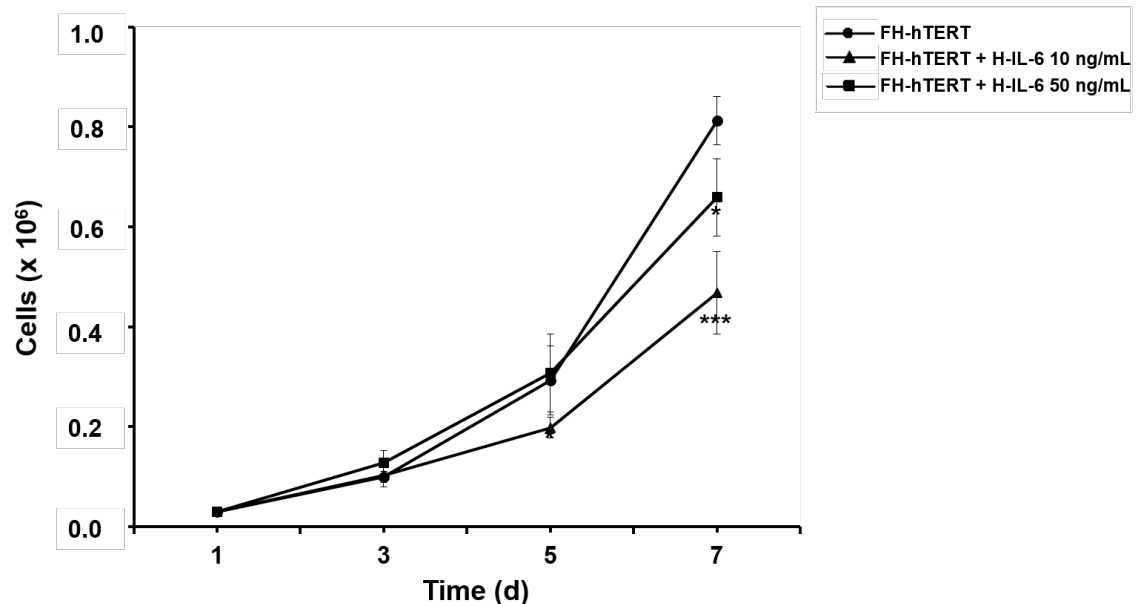

Figure 15. Cell proliferation of FH-hTERT incubated with Hyper-IL-6. Each time point represents the mean of 4 independent cell counts. *P*-values are as indicated, *P*<0.05 (*), *P*<0.001 (***).

In FH-hTERT incubated with both concentrations of Hyper-IL-6, cells showed a reduced proliferation in comparison to control cells. The difference between Hyper-IL-6 incubated cells and untreated cells was statistically significant.

5.3.3. ROS detection

To investigate the oncogenic potential of oxidative stress in FH-hTERT with gp130-activation, we induced ROS by treating the L-gp130 clones with H_2O_2/BSO. Interestingly, challenge with oxidative stress induced higher ROS levels in comparison to the control cells. To compare ligand-independent to ligand-dependent IL-6 activation, we incubated FH-hTERT with Hyper-IL-6 and measured ROS activation after treatment with H_2O_2/BSO (Figure 16).
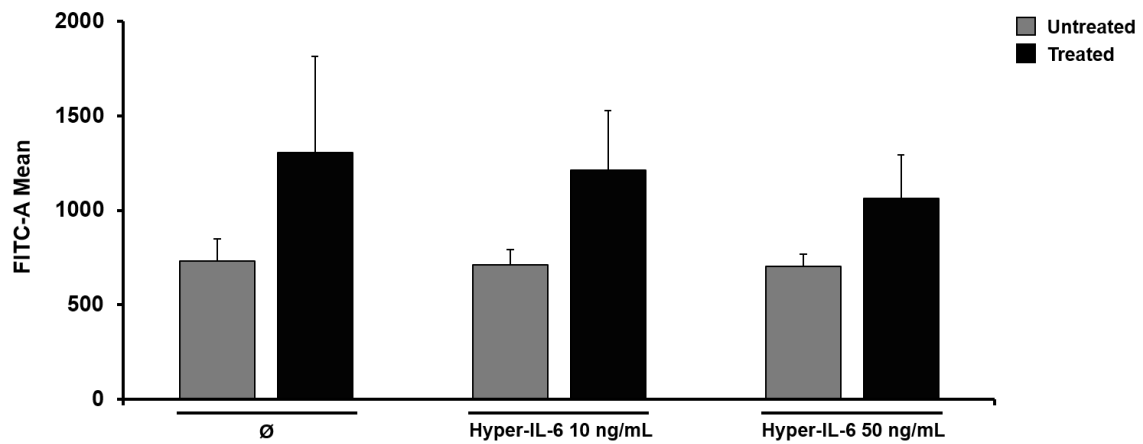
Figure 16. Levels of ROS in FH-hTERT with IL-6 signaling activation by Hyper-IL-6. ROS levels (y-axis; FITC-A mean) of untreated cells (■) are compared to ROS levels after H_2O_2/BSO treatment (■).

There was no difference between ROS-untreated FH-hTERT and Hyper-IL-6-incubated FH-hTERT without ROS challenge (FITC-A mean: Ø 732 ± 118; Hyper-IL-6 10 ng/ml 713 ± 79; Hyper-IL-6 50 ng/ml 703 ± 66). In contrast to L-gp130 clones, H_2O_2/BSO treatment did not result in higher ROS levels in Hyper-IL-6-actived cells compared to ROS-treated FH-hTERT control cells (FITC-A mean: Ø 1306 ± 507; Hyper-IL-6 10 ng/ml 1212 ± 317; Hyper-IL-6 50 ng/ml 1061 ± 231).

5.3.4. DNA synthesis rate

Newly synthesized DNA was also measured in Hyper-IL-6-incubated FH-hTERT cells after ROS challenge by determining S-phase fractions by BrdU-incorporation and FACS quantification (Figure 17).
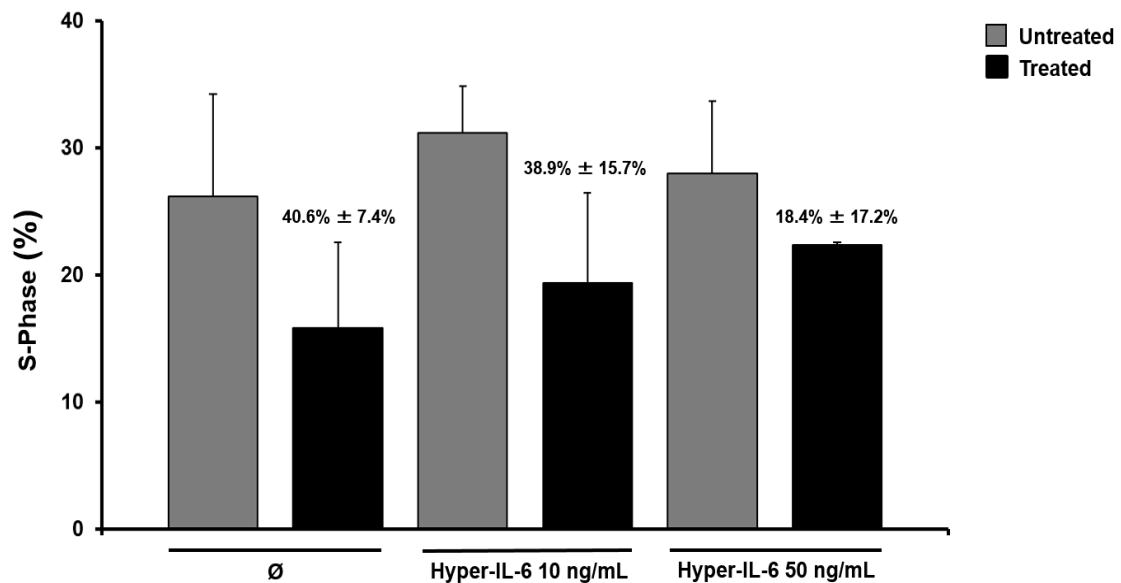
Figure 17. S-phase analysis under oxidative stress determined by BrdU incorporation assay. The bars represent the average S-phase fractions and the calculated S-phase reduction in % ± SD (error bars) of untreated (■) and treated (■) cells.

In contrast to FH-hTERT L-gp130 clone 1-3, we did not detect differences in cell cycle arrest between Hyper-IL-6-actived cells and the control cells after ROS challenge. Both, FH-hTERT and Hyper-IL-6-activated FH-hTERT showed reduction in S-Phase. FH-hTERT showed the highest suppression in S-phase with a 40.6% ± 7.4% reduction. In FH-hTERT incubated with Hyper-IL-6 (10 ng/mL and 50 ng/mL), S-phase was reduced by 38.9% ± 15.7% and 18.4% ± 17.2%, respectively.

6. Discussion

Inflammation is a normal body response to harmful stimuli; but, if inflammation becomes chronic, it facilitates the emergence of several pathologies, including cancer. Chronic infection and unresolved inflammation are associated with over 25% of all cancers, especially liver cancer [72]. HCC is one of the most prevalent inflammation-associated human malignancy with more than 90% of all cases arising in the context of chronic hepatic injury and inflammation [73]. Nonetheless, the molecular and cellular mechanisms interconnecting inflammatory pathways and cancer development are not completely understood [74].

Inflammatory cytokines, such as IL-6, have already been identifed as initial and key players in multi-step tumorigenesis [75]. Regarding HCC, a high IL-6 serum level is described as a prognostic indicator for disease progression. Therefore, its inhibition could be an interesting therapeutic target [76]. Furthermore, IL-6 has been identified as an independent risk factor for the development of HCC in patients with chronic hepatitis B and it is linked to the transition from chronic viral hepatitis to HCC [25], [24]. Based on these observations, IL-6 and the pro-inflammatory downstream signaling pathways are currently a focus of intense scientific research.

In order to elucidate the driving oncogenic mechanisms of IL-6 signaling activation in human hepatocytes, we stably transfected telomerase-immortalized human fetal hepatocytes (FH-hTERT) [11] with the constitutively active L-gp130 construct [47] in a previous project. Thereby, clones with constant IL-6 pathway activation independent of the presence of IL-6 were generated.

6.1. Characterization of constitutive gp130 activation

Previously, cancer-associated growth properties, such as serum dependence, contact inhibition, and colony formation were monitored in FH-hTERT L-gp130 clones. Bollrath *et al.* described gp130-mediated signaling as promoter bridging chronic inflammation and tumor formation [77]. In agreement with this description, our data showed a less serum-sensitive cell growth, and decreased contact inhibition in FH-hTERT with constitutive gp130 activation. Moreover, colony formation in soft agar, an established *in vitro* indicator for malignant transformation, developed in all three L-gp130 clones during long-term expansion culture. Corresponding to the colony assay data, two of the three transplanted clones (clone 1 and clone 3) formed subcutaneous tumors in athymic nude mice after a latency period of 8 to 10 weeks. However, forced gp130 activation was not sufficient to induce an immediate full transformation in our clones. Instead, constitutive gp130 activation promoted the transformation process in FH-hTERT during additional rounds of cell turnover in long-term culture or following subcutaneous transplantation. In summary, our L-gp130 clones displayed a pre-malignant phenotype with tumor growth characteristics, but other mediators are needed to induce full malignant transformation. In line with this observation, gp130 was described by Hatting *et al.* as driver of HCC progression, but on the other hand, as an unnecessary factor for HCC initiation [78]. Another study showed that in HCC with gp130 mutations an additional activating mutation in the β-catenin pathway is frequently present, again indicating that additional genetic hits are required for malignant transformation of hepatocytes with gp130 activation [45].

6.2. Oxidative stress accelerates malignant transformation

ROS activate various signaling cascades that regulate cell growth and transformation [79], and are currently discussed as trigger for inflammation-mediated carcinogenesis [80]. In the case of viral hepatitis, a strong connection

between chronic infection and induction of oxidative stress has been established. Furthermore, different groups have also associated other viral infections with increased oxidative stress, DNA damage, and a high mutagenic rate [81].

To study the oncogenic potential of oxidative stress in our cell culture model, L-gp130 clones were subsequently treated with H_2O_2/BSO. Interestingly, challenge with oxidative stress resulted in up to 3-fold higher ROS levels in our clones compared to ROS-treated FH-hTERT control cells. In the clinical setting, higher ROS levels in the liver have been linked to increased cancer risk without clearly defining the specific ROS-mediated mechanisms [82]. To identify the gp130-related mechanisms leading to higher ROS levels in our clones following oxidative stress induction, we profiled the expression of antioxidative defence genes in untreated clones. Despite similar ROS levels, we detected a significantly altered expression of GPX3, CYGB, APOE, DHCR24, and SEPP1 in our L-gp130 clones compared to the control cells. Based on these findings, we conclude that an altered gp130-mediated oxidative stress response is a possible mechanism for the observed increase in ROS levels. Deng *et al*. reported that the downregulation of ROS inhibited colony formation in intrahepatic cholangiocarcinoma cells [83]. A pro-malignant role of ROS was also described in breast cancer, where estrogen-induced ROS was identified as promoter of *in vitro* cell transformation. Having these results in mind, we challenged our L-gp130 clones in early expansion culture (pre-malignant phenotype without colony formation in soft agar) with oxidative stress and monitored phenotype changes by soft agar assay in the present study. In contrast to the previous study, the transformation process observed in long-term culture (see above) was significantly accelerated after challenge with ROS and colony formation was detected directly after H_2O_2/BSO treatment.

6.3. Mechanisms of ROS-induced transformation

In order to dissect the gp130-induced mechanisms underlying the accelerated transformation in our clones, we assessed the expression of antioxidant response genes by qPCR, DNA-damage by visualizing DSB by immunofluorescent staining for γ-H2AX, and DSB-altered cell cycling by the measurement of BrdU incorporation.

6.3.1. Altered antioxidative defense after ROS challenge

Considering the previous study that showed modified expression of GPX3, CYGB, SOD3, APOE, DHCR24, and SEPP1 in our untreated clones [48], we decided to determine the expression levels of these genes after ROS challenge, as well as the expression of the antioxidative transcription gene NQO1. NQO1 is one of the target genes of NRF2, which has been described as the principal regulator of cytoprotective and antioxidant genes in several carcinogenesis processes, e.g. ovarian cancer [84].

GPX3 showed a downregulation after 7 and 12 hours incubation with ROS. It is known that GPX3 is the most important ROS scavenger [85] and its expression is suppressed in a variety of cancers. The expression of GPX3 in HCC has not been studied, but our data suggest a correlation between gp130 activation and decreased GPX3 expression in the context of oxidative stress. In contrast, CYGB expression was robustly increased after 7 hours with up to 10-fold higher expression levels in ROS-treated clone 3 compared to ROS-treated FH-hTERT contol cells. This increase was slightly reduced after 12 hours showing clone 3 with a 3-fold upregulation in comparison to ROS-treated FH-hTERT cells. CYGB overexpression seems to protect the cells from pro-oxidant induced DNA damage [86]. Le *et al*. suggested that CYGB deficiency induces susceptibility to cancer development in the liver and lungs of mice exposed to *N,N*-diethylnitrosamine [87]. SOD3, an extracellular member of the SOD family, reduces degradation of superoxide into oxygen and hydrogen peroxide

protecting cells against oxidative stress [88]. In our cell culture system, FH-hTERT L-gp130 clones showed a reduction in the expression of SOD3 suggesting an increased production of ROS. Yokoyama *et al.* reported increased APOE protein levels in 88% of HCC patients, but without upregulation in APOE gene expression and serum levels, thus suggesting an accumulation by impaired secretion [89]. In our gp130-activated clones, a robust decrease in APOE expression was observed after 7 and 12 hours H_2O_2/BSO treatment. High levels of the oxidoreductase DHCR24 mediate resistance against oxidative stress and prevent apoptotic cell death [90]. In our immortalized clones, we observed a downregulation of DHCR24 expression after 7 hours and 12 hours treatment compared to the ROS-treated control cells. In the case of SEPP1, a reduced expression has been detected in prostate tumors and colon cancers [91], [92]. Regarding HCC, a study showed that SEPP1-mRNA expression in normal liver and HCC is significantly different (84.6% *versus* 30.0%), suggesting that SEPP1 might play a role in the occurrence and development of HCC [93]. In our cell culture system, clones with gp130 activation showed a remarkable reduction in the expression of SEPP1 after 7 hours ROS challenge compared to ROS-treated control cells. This reduction is even more distinct after 12 hours oxidative stress treatment. The transcription factor NRF2 restores redox homeostasis but its activity cannot directly be quantified. Therefore, markers such as the target gene NQO1 are needed to determine NRF2-response. As corroboration of this NRF2-NQO1 link Liang *et al.* demonstrated that the stimulation of NRF2-dependent signaling by dihydroquercetin, a well-known antioxidant agent, induces an upregulation of NQO1 [94]. In regard of HCC, a meta-analysis suggested that NQO1 variant alleles and genotypes were significantly related to an increased risk of tumor development [95]. Our L-gp130 clones showed an upregulated NQO1 expression following 7 and 12 hours incubation with ROS in comparison to the treated control cells and as expected. In conclusion, our data indicate that ROS treatment alters the oxidative stress response in our L-gp130 clones, particularly by disturbing the expression of GPX3, SOD3, DHCR24, and SEPP1.

6.3.2. Increased genomic instability after ROS challenge

To assess oxidative stress-induced genomic alterations, we tested if the higher ROS levels result in more DNA damage by visualizing DSB by immunofluorescent staining for γ-H2AX [96]. After H_2O_2/BSO treatment, a significant up to 3-fold increase in the number of γ-H2AX foci was detected in our L-gp130 clones, indicating extensively more DSB compared to ROS-treated FH-hTERT control cells. It has already been reported that various HCC-associated risk factors are able to promote DNA damage, formation of DNA adducts, and chromosomal aberrations, and ROS seem to be one of them [97].

6.3.3. Absent cell cycle arrest after ROS challenge

Normally, DSB activate the DNA damage response machinery that in turn leads to cell cycle arrest, DNA repair, and apoptosis. To examine DSB-induced cell cycle control mechanisms in our L-gp130 clones, S-Phase fractions were determined by the measurement of BrdU incorporation. Untreated clones showed similar proliferation rates compared to untreated control cells. However, L-gp130 clones displayed an increase in S-phase fraction after H_2O_2/BSO treatment in comparison to ROS-treated control cells. Taken together, our data showed that our treated L-gp130 clones did not enter cell cycle arrest after ROS challenge and even displayed an enhanced proliferation despite higher ROS and DSB levels. These findings are supported by a study from Trachootham *et al.* suggesting that a moderate increment of ROS levels promotes cell proliferation, and also, that cells with increased oxidative stress are probably more vulnerable to damage by further ROS insults [98].

In summary, our findings allowed us to conclude that a forced activation of IL-6 signaling via gp130 directly alters the oxidative stress response, causing higher ROS levels, and subsequently a higher frequency of DSB after oxidative stress treatment. In addition, enhanced cell cycle turnover driven by gp130 activation associated with ROS challenge leads to the accumulation of unrepaired DSB

and subsequently to genomic aberrations, finally resulting in the transformation of our L-gp130 clones. Together with others studies [99], these results support the possible role of ROS as target for anticancer therapies. These ROS-manipulating therapies, called redox-modulating drugs, are currently under investigation in various clinical trials [100]. For example, Fan *et al.* study the combination of doxorubicin-based chemotherapy with selenocystine, an agent that controls ROS-mediated DNA-damage, and propose the combination as new therapy for HCC [101].

6.4. Ligand-dependent IL-6 signaling activation via Hyper-IL-6

To compare ligand-independent to ligand-dependent IL-6 pathway activation, we treated FH-hTERT with the designer cytokine Hyper-IL-6. Following incubation with Hyper-IL-6, IL-6 signaling activation was confirmed in FH-hTERT cells by immunoblotting STAT-3 phosphorylation.

6.4.1. Proliferation

Proliferation of FH-hTERT L-gp130 clones and FH-hTERT incubated with Hyper-IL-6 was measured by cell counts. Regarding L-gp130 clones, only clone 3 presented an increased proliferation rate compared to FH-hTERT. In the case of Hyper-IL-6 incubated cells, proliferation was always lower than in the control cells with a significant difference from day five on. No difference was seen between 10 and 50 ng/ml Hyper-IL-6. In contrast to our data, Hyper-IL-6 seems to have the ability to stimulate proliferation in other liver cell lines, e.g. L-02 [102], as well as in plasmacytoma cells [103]. Therefore, we speculate that Hyper-IL-6 incubation of FH-hTERT cells resulted only in a short-term activation and the proliferation stimulus is not sufficient.

6.4.2. ROS challenge

To evaluate the impact of genetic gp130-mediated activation of IL-6 signaling in our cell system in comparison to ligand activation, we recapitulated our experiments following ROS challenge in FH-hTERT cells incubated with Hyper-IL-6. In contrast to our L-gp130 clones with genetically driven gp130 activation, H_2O_2/BSO treatment did not result in higher ROS levels in Hyper-IL-6-activated cells in comparison to ROS-treated FH-hTERT control cells. Moreover, cells treated with 10 and 50 ng/ml Hyper-IL-6 showed lower ROS levels than the control cells. Considering that higher ROS levels were observed in all three ROS-treated L-gp130 clones compared to ROS-treated FH-hTERT, we speculate that Hyper-IL-6 did not alter ROS defense. In addition, DSB-induced cell cycle control mechanisms were examined by determining S-Phase fractions in Hyper-IL-6-acivated FH-hTERT cells after ROS challenge. In contrast to the L-gp130 clones, FH-hTERT cells incubated with Hyper-IL-6 showed decreased proliferation following ROS challenge, similar to the cells without IL-6 activation. Thus, FH-hTERT activated by Hyper-IL-6 enter cell cycle arrest after H_2O_2/BSO treatment. Furthermore, no difference was detected between 10 and 50 ng/ml treatment. Therefore, we conclude that under Hyper-IL-6 incubation FH-hTERT cells are still able to repair DNA-damage caused by oxidative stress and that Hyper-IL-6 is not sufficient to induce a pre-malignant phenotype.

6.5. L-gp130 *versus* Hyper-IL-6

FH-hTERT L-gp130 clones as well as FH-hTERT cells incubated with Hyper-IL-6 showed active IL-6 signaling. However, our data show remarkable differences between ligand-dependent and ligand-independent IL-6 pathway activation. It is important to highlight that incubation with Hyper-IL-6 may only achieve a short-term IL-6 signaling activation. In contrast, following L-gp130 transfection, FH-hTERT cells acquired uninterrupted pro-inflammatory IL-6 pathway activation. Based on these considerations, we conclude that in contrast to L-gp130 clones,

ROS defense does not seem to be permanently altered or not altered at all in FH-hTERT cells incubated with Hyper-IL-6. ROS levels after oxidative stress increased in the same extent than in the ROS-treated control cells. Moreover, a decreased proliferation was observed in FH-hTERT incubated with Hyper-IL-6 indicating a normal cell cycle arrest after oxidative stress treatment. These findings contradict Peters *et al.*, who observed an earlier and accelerated liver regeneration after partial hepatectomy in mice treated with Hyper-IL-6 [104].

In summary, we propose that Hyper-IL-6 activation is not sufficient to alter oxidative stress response in the same extend as constitutive gp130 activation. In addition, Hyper-IL-6 is not sufficient to force the required cell cycle turnover for full transformation. Nonetheless, repeated Hyper-IL-6 treatments could be sufficient to reach cellular malignant transformation. On the other hand, permanent genetically driven IL-6 signaling activation promotes transformation by pushing pre-malignant cells with genetic alterations through additional cell cycle rounds. In fact, gp130 mutations have been associated with several malignant processes, e.g., the development of HCC from inflammatory hepatocellular adenomas [105].

We have to point out that our human cell culture model is limited to the investigation of cellular mechanisms and further investigations in more complex systems including the immune system have to be conducted. A better understanding of the mechanisms of ligand-dependent in comparison to genetic activation of IL-6 signaling in hepatocytes could result in novel and highly targeted therapeutic options.

7. Summary

The present study established that oxidative stress accelerates the transformation of FH-hTERT with constitutive gp130 activation in contrast to ligand-dependent IL-6 signaling activation via Hyper-IL-6. Forced gp-130 activation instigated our FH-hTERT cells to a pre-malignant phenotype with cancer-associated growth capabilities. Nevertheless, oxidative stress is needed to achieve a full malignant transformation. Interestingly, oxidative stress resulted in higher ROS levels and an increased number of DSB in our L-gp130 clones, possibly via an altered gp130-mediated oxidative stress response. An enhanced cell cycle turnover in gp130-active cells may additionally result in the accumulation of unrepaired DSB, and finally in cellular transformation recognized by colony formation capability. In contrast, incubation with the designer cytokine Hyper-IL-6 did not result in an enhanced proliferation. Moreover, no changes in ROS levels were observed after Hyper-IL-6 incubation. Therefore, we conclude that unlike in Hyper-IL-6-actived cells, ROS induced transformation in FH-hTERT with gp130-activation by driving these pre-malignant cells with altered oxidative stress response through additional cell cycle rounds.

8. Abbreviations

APC-A	allophycocyanin A
APOE	apolipoprotein E
BCA	bicinchoninic acid
BrdU	5-bromodeoxyuridine
BSA	bovine serum albumin
BSO	DL-buthionine-[S,R]-sulfoximine
B2M	ß-2-microglobulin
Carboxy-DCF	carboxy-dichlorofluorescen
Carboxy-H_2DCFDA	5-(6)-carboxy-2´,7´-dichlorodihydrofluorescein diacetate
CDK	cyclin-dependent kinase
cDNA	complementary deoxyribonucleic acid
CO_2	carbon dioxide
Ct	cycle number at threshold
CYGB	cytoglobin
CYP450	cytochrome P540
DHCR24	24-dehydrocholesterol reductase
DMEM	Dulbecco's Modified Eagle Medium
DNA	deoxyribonucleic acid
DSB	DNA-double strand breaks
EDTA	ethylenediaminetetraacetic acid
EMT	epithelial-mesenchymal transition
ERK	extracellular signal-regulated kinase
FACS	fluorescence activated cell sorting
FBS	fetal bovine serum
FH-hTERT	telomerase reverse transcriptase-transduced human fetal hepatocytes
γ-H2AX	gamma-H2A histone family, member X
GAPDH	glycernaldehyde-3-phosphate-dehydrogenase

GPX3	glutathione peroxidase 3
gp130	IL-6 signal-transducing glycoprotein 130
HBSS	Hank's Balanced Salt Solution
HCC	hepatocellular carcinoma
HepG2	human hepatoblastom cell line
hTERT	human telomerase reverse transcriptase
Hyper-IL-6	hyper interleukin 6
H2AX	H2A histone family, member X
H_2O_2	hydrogen peroxide
IL-6	interleukin 6
IL-6R	interleukin-6 receptor
JAK	janus kinase
kDa	kilo Dalton
L-gp130	constitutively active gp130
NMRI	Naval Medical Research Institute
NQO1	NAD(P)H dehydrogenase quinone 1
NRF2	nuclear factor (erythroid-derived 2)-like 2
PAGE	polyacrylamide gel electrophoresis
PBS	phosphate buffered saline
PD	population doubling
PCR	polymerase chain reaction
PI3K	phosphoinositide 3-kinase
PTEN	phosphatase and tensin homolog
p-ERK	phosphorylated extracellular signal-regulated kinase
p-STAT3	phosphorylated signal transducer and activator of transcription–3
p21	cyclin-dependent kinase inhibitor 1A
p53	tumor protein 53
qPCR	quantitative real-time PCR
Rad51	RAD51 recombinase
Rb	retinoblastoma protein
rDNase	recombinant deoxyribonuclease

RIPA	radioimmunoprecipitation assay
RNA	ribonucleic acid
RNase	ribonuclease
ROS	reactive oxygen species
RPL13A	ribosomal protein L13a
SD	standard deviation
SDS	sodium dodecyl sulphate
SEPP1	selenoprotein P 1
SH2	Src homology 2
SHP-2	protein tyrosine phosphatase-2
sIL-6R	soluble interleukin-6 receptor
SOD3	superoxide dismutase 3
STAT3	signal transducer and activator of transcription – 3
$^-$OH	hydroxyl radical
TE	Tris and EDTA
TBP	TATA-box binding protein
TBST	Tris-buffered saline and Tween 20
7-AAD	7-aminoactinomycin D

9. LIST OF TABLES AND FIGURES

Table:

Figures:

10. Bibliography

1.   Wong, V.W. and H.L. Chan, *Prevention of hepatocellular carcinoma: a concise review of contemporary issues.* Ann Hepatol, 2012. **11**(3): p. 284-93.

2.   Maluccio, M. and A. Covey, *Recent progress in understanding, diagnosing, and treating hepatocellular carcinoma.* CA Cancer J Clin, 2012. **62**(6): p. 394-9.

3.   El-Serag, H.B., *Epidemiology of viral hepatitis and hepatocellular carcinoma.* Gastroenterology, 2012. **142**(6): p. 1264-1273 e1.

4.   Aghemo, A. and M. Colombo, *Hepatocellular carcinoma in chronic hepatitis C: from bench to bedside.* Semin Immunopathol, 2013. **35**(1): p. 111-20.

5.   Gao, J., et al., *Risk factors of hepatocellular carcinoma--current status and perspectives.* Asian Pac J Cancer Prev, 2012. **13**(3): p. 743-52.

6.   Roberts, L.R. and G.J. Gores, *Hepatocellular carcinoma: molecular pathways and new therapeutic targets.* Semin Liver Dis, 2005. **25**(2): p. 212-25.

7.   Thelen, A., et al., *Liver resection for hepatocellular carcinoma in patients without cirrhosis.* Br J Surg, 2013. **100**(1): p. 130-7.

8.   Naugler, W.E. and J.M. Schwartz, *Hepatocellular carcinoma.* Dis Mon, 2008. **54**(7): p. 432-44.

9.   Pfeiffer, E., et al., *Isolation, characterization, and cultivation of human hepatocytes and non-parenchymal liver cells.* Exp Biol Med (Maywood), 2014.

10.   Nyberg, S.L., et al., *Primary hepatocytes outperform Hep G2 cells as the source of biotransformation functions in a bioartificial liver.* Ann Surg, 1994. **220**(1): p. 59-67.

11.   Wege, H., et al., *Telomerase reconstitution immortalizes human fetal hepatocytes without disrupting their differentiation potential.* Gastroenterology, 2003. **124**(2): p. 432-44.

12.   Shay, J.W., O.M. Pereira-Smith, and W.E. Wright, *A role for both RB and p53 in the regulation of human cellular senescence.* Exp Cell Res, 1991. **196**(1): p. 33-9.

13. Kim, N.W., et al., *Specific association of human telomerase activity with immortal cells and cancer.* Science, 1994. **266**(5193): p. 2011-5.

14. Wege, H. and T.H. Brummendorf, *Telomerase activation in liver regeneration and hepatocarcinogenesis: Dr. Jekyll or Mr. Hyde?* Curr Stem Cell Res Ther, 2007. **2**(1): p. 31-8.

15. Shay, J.W. and S. Bacchetti, *A survey of telomerase activity in human cancer.* Eur J Cancer, 1997. **33**(5): p. 787-91.

16. Haker, B., et al., *Absence of oncogenic transformation despite acquisition of cytogenetic aberrations in long-term cultured telomerase-immortalized human fetal hepatocytes.* Cancer Lett, 2007. **256**(1): p. 120-7.

17. Villanueva, A. and J.M. Llovet, *Targeted therapies for hepatocellular carcinoma.* Gastroenterology, 2011. **140**(5): p. 1410-26.

18. Bishayee, A., *The role of inflammation and liver cancer.* Adv Exp Med Biol, 2014. **816**: p. 401-35.

19. Weber, A., et al., *Chronic liver inflammation and hepatocellular carcinoma: persistence matters.* Swiss Med Wkly, 2011. **141**: p. w13197.

20. Aravalli, R.N., E.N. Cressman, and C.J. Steer, *Cellular and molecular mechanisms of hepatocellular carcinoma: an update.* Arch Toxicol, 2013. **87**(2): p. 227-47.

21. Ataie-Kachoie, P., et al., *Gene of the month: Interleukin 6 (IL-6).* J Clin Pathol, 2014. **67**(11): p. 932-7.

22. Multhoff, G., M. Molls, and J. Radons, *Chronic inflammation in cancer development.* Front Immunol, 2011. **2**: p. 98.

23. Taniguchi, K. and M. Karin, *IL-6 and related cytokines as the critical lynchpins between inflammation and cancer.* Semin Immunol, 2014. **26**(1): p. 54-74.

24. Nakagawa, H., et al., *Serum IL-6 levels and the risk for hepatocarcinogenesis in chronic hepatitis C patients: an analysis based on gender differences.* Int J Cancer, 2009. **125**(10): p. 2264-9.

25. Wong, V.W., et al., *High serum interleukin-6 level predicts future hepatocellular carcinoma development in patients with chronic hepatitis B.* Int J Cancer, 2009. **124**(12): p. 2766-70.

26. Johnson, C., et al., *Interleukin-6 and its receptor, key players in hepatobiliary inflammation and cancer.* Transl Gastrointest Cancer, 2012. **1**(1): p. 58-70.

27. Malaguarnera, M., et al., *[Role of interleukin 6 in hepatocellular carcinoma].* Bull Cancer, 1996. **83**(5): p. 379-84.

28. May, P., et al., *Signal transducer and activator of transcription STAT3 plays a major role in gp130-mediated acute phase protein gene activation.* Acta Biochim Pol, 2003. **50**(3): p. 595-601.

29. Yu, H., D. Pardoll, and R. Jove, *STATs in cancer inflammation and immunity: a leading role for STAT3.* Nat Rev Cancer, 2009. **9**(11): p. 798-809.

30. Yu, H., M. Kortylewski, and D. Pardoll, *Crosstalk between cancer and immune cells: role of STAT3 in the tumour microenvironment.* Nat Rev Immunol, 2007. **7**(1): p. 41-51.

31. Johnston, P.A. and J.R. Grandis, *STAT3 signaling: anticancer strategies and challenges.* Mol Interv, 2011. **11**(1): p. 18-26.

32. Haricharan, S. and Y. Li, *STAT signaling in mammary gland differentiation, cell survival and tumorigenesis.* Mol Cell Endocrinol, 2014. **382**(1): p. 560-9.

33. Giraud, A.S., T.R. Menheniott, and L.M. Judd, *Targeting STAT3 in gastric cancer.* Expert Opin Ther Targets, 2012. **16**(9): p. 889-901.

34. Zhang, D. and T.P. Loughran, Jr., *Large granular lymphocytic leukemia: molecular pathogenesis, clinical manifestations, and treatment.* Hematology Am Soc Hematol Educ Program, 2012. **2012**: p. 652-9.

35. He, G., et al., *Hepatocyte IKKbeta/NF-kappaB inhibits tumor promotion and progression by preventing oxidative stress-driven STAT3 activation.* Cancer Cell, 2010. **17**(3): p. 286-97.

36. Liu, R.Y., et al., *Association between IL6 -174G/C and cancer: A meta-analysis of 105,482 individuals.* Exp Ther Med, 2012. **3**(4): p. 655-664.

37. Lin, Z.Y., Y.H. Chuang, and W.L. Chuang, *Cancer-associated fibroblasts up-regulate CCL2, CCL26, IL6 and LOXL2 genes related to promotion of cancer progression in hepatocellular carcinoma cells.* Biomed Pharmacother, 2012. **66**(7): p. 525-9.

38. Wan, S., et al., *Tumor-associated macrophages produce interleukin 6 and signal via STAT3 to promote expansion of human hepatocellular carcinoma stem cells.* Gastroenterology, 2014. **147**(6): p. 1393-404.

39. Wolf, J., S. Rose-John, and C. Garbers, *Interleukin-6 and its receptors: a highly regulated and dynamic system.* Cytokine, 2014. **70**(1): p. 11-20.

40.   Scheller, J., et al., *The pro- and anti-inflammatory properties of the cytokine interleukin-6.* Biochim Biophys Acta, 2011. **1813**(5): p. 878-88.

41.   Rose-John, S., *IL-6 trans-signaling via the soluble IL-6 receptor: importance for the pro-inflammatory activities of IL-6.* Int J Biol Sci, 2012. **8**(9): p. 1237-47.

42.   Rose-John, S., et al., *The IL-6/sIL-6R complex as a novel target for therapeutic approaches.* Expert Opin Ther Targets, 2007. **11**(5): p. 613-24.

43.   Jones, S.A., et al., *IL-6 transsignaling: the in vivo consequences.* J Interferon Cytokine Res, 2005. **25**(5): p. 241-53.

44.   Scheller, J., C. Garbers, and S. Rose-John, *Interleukin-6: from basic biology to selective blockade of pro-inflammatory activities.* Semin Immunol, 2014. **26**(1): p. 2-12.

45.   Rebouissou, S., et al., *Frequent in-frame somatic deletions activate gp130 in inflammatory hepatocellular tumours.* Nature, 2009. **457**(7226): p. 200-4.

46.   Taga, T. and T. Kishimoto, *Gp130 and the interleukin-6 family of cytokines.* Annu Rev Immunol, 1997. **15**: p. 797-819.

47.   Stuhlmann-Laeisz, C., et al., *Forced dimerization of gp130 leads to constitutive STAT3 activation, cytokine-independent growth, and blockade of differentiation of embryonic stem cells.* Mol Biol Cell, 2006. **17**(7): p. 2986-95.

48.   Herden, J.R., *Relevanz der konstitutiven Aktivierung des IL-6-Signalwegs für die Proliferation und Transformation humaner Leberzellen* 2014. http://ediss.sub.uni-hamburg.de/volltexte/2014/6852/

49.   Ray, P.D., B.W. Huang, and Y. Tsuji, *Reactive oxygen species (ROS) homeostasis and redox regulation in cellular signaling.* Cell Signal, 2012. **24**(5): p. 981-90.

50.   Waris, G. and H. Ahsan, *Reactive oxygen species: role in the development of cancer and various chronic conditions.* J Carcinog, 2006. **5**: p. 14.

51.   Tien Kuo, M. and N. Savaraj, *Roles of reactive oxygen species in hepatocarcinogenesis and drug resistance gene expression in liver cancers.* Mol Carcinog, 2006. **45**(9): p. 701-9.

52.   Da Costa, L.A., A. Badawi, and A. El-Sohemy, *Nutrigenetics and modulation of oxidative stress.* Ann Nutr Metab, 2012. **60 Suppl 3**: p. 27-36.

53. Stadler, K., *Oxidative stress in diabetes.* Adv Exp Med Biol, 2012. **771**: p. 272-87.

54. Wong, B.W., et al., *The biological role of inflammation in atherosclerosis.* Can J Cardiol, 2012. **28**(6): p. 631-41.

55. Ivanov, A.V., et al., *HCV and oxidative stress in the liver.* Viruses, 2013. **5**(2): p. 439-69.

56. Porter, K.M. and R.L. Sutliff, *HIV-1, reactive oxygen species, and vascular complications.* Free Radic Biol Med, 2012. **53**(1): p. 143-59.

57. Kipanyula, M.J., et al., *Signaling pathways bridging microbial-triggered inflammation and cancer.* Cell Signal, 2013. **25**(2): p. 403-16.

58. Fausto, N. and J.S. Campbell, *Mouse models of hepatocellular carcinoma.* Semin Liver Dis, 2010. **30**(1): p. 87-98.

59. Gupta, S.C., et al., *Upsides and downsides of reactive oxygen species for cancer: the roles of reactive oxygen species in tumorigenesis, prevention, and therapy.* Antioxid Redox Signal, 2012. **16**(11): p. 1295-322.

60. Peters, M., et al., *In vivo and in vitro activities of the gp130-stimulating designer cytokine Hyper-IL-6.* J Immunol, 1998. **161**(7): p. 3575-81.

61. Sansone, P. and J. Bromberg, *Targeting the interleukin-6/Jak/stat pathway in human malignancies.* J Clin Oncol, 2012. **30**(9): p. 1005-14.

62. Eulenfeld, R., et al., *Interleukin-6 signalling: more than Jaks and STATs.* Eur J Cell Biol, 2012. **91**(6-7): p. 486-95.

63. Huang, T., M. Long, and B. Huo, *Competitive Binding to Cuprous Ions of Protein and BCA in the Bicinchoninic Acid Protein Assay.* Open Biomed Eng J, 2010. **4**: p. 271-8.

64. Towbin, H., T. Staehelin, and J. Gordon, *Electrophoretic transfer of proteins from polyacrylamide gels to nitrocellulose sheets: procedure and some applications. 1979.* Biotechnology, 1992. **24**: p. 145-9.

65. Davidson, B., et al., *The diagnostic and research applications of flow cytometry in cytopathology.* Diagn Cytopathol, 2012. **40**(6): p. 525-35.

66. Ichiseki, T., et al., *Oxidative stress by glutathione depletion induces osteonecrosis in rats.* Rheumatology (Oxford), 2006. **45**(3): p. 287-90.

67. Engel, R.H. and A.M. Evens, *Oxidative stress and apoptosis: a new treatment paradigm in cancer.* Front Biosci, 2006. **11**: p. 300-12.

68. Xue, L., et al., *Structurally dependent redox property of ribonucleotide reductase subunit p53R2.* Cancer Res, 2006. **66**(4): p. 1900-5.

69. Valko, M., et al., *Role of oxygen radicals in DNA damage and cancer incidence.* Mol Cell Biochem, 2004. **266**(1-2): p. 37-56.

70. Koch, K., et al., *Impact of homologous recombination on individual cellular radiosensitivity.* Radiother Oncol, 2009. **90**(2): p. 265-72.

71. Fleige, S., et al., *Comparison of relative mRNA quantification models and the impact of RNA integrity in quantitative real-time RT-PCR.* Biotechnol Lett, 2006. **28**(19): p. 1601-13.

72. Vendramini-Costa, D.B. and J.E. Carvalho, *Molecular link mechanisms between inflammation and cancer.* Curr Pharm Des, 2012. **18**(26): p. 3831-52.

73. Nakagawa, H. and S. Maeda, *Inflammation- and stress-related signaling pathways in hepatocarcinogenesis.* World J Gastroenterol, 2012. **18**(31): p. 4071-81.

74. Okada, F., *Inflammation-related carcinogenesis: current findings in epidemiological trends, causes and mechanisms.* Yonago Acta Med, 2014. **57**(2): p. 65-72.

75. Alison, M.R., L.J. Nicholson, and W.R. Lin, *Chronic inflammation and hepatocellular carcinoma.* Recent Results Cancer Res, 2011. **185**: p. 135-48.

76. Ataie-Kachoie, P., M.H. Pourgholami, and D.L. Morris, *Inhibition of the IL-6 signaling pathway: a strategy to combat chronic inflammatory diseases and cancer.* Cytokine Growth Factor Rev, 2013. **24**(2): p. 163-73.

77. Bollrath, J., et al., *gp130-mediated Stat3 activation in enterocytes regulates cell survival and cell-cycle progression during colitis-associated tumorigenesis.* Cancer Cell, 2009. **15**(2): p. 91-102.

78. Hatting, M., et al., *Lack of gp130 expression in hepatocytes attenuates tumor progression in the DEN model.* Cell Death Dis, 2015. **6**: p. e1667.

79. Finkel, T. and N.J. Holbrook, *Oxidants, oxidative stress and the biology of ageing.* Nature, 2000. **408**(6809): p. 239-47.

80. Kamp, D.W., E. Shacter, and S.A. Weitzman, *Chronic inflammation and cancer: the role of the mitochondria.* Oncology (Williston Park), 2011. **25**(5): p. 400-10, 413.

81. Georgakilas, A.G., et al., *Viral-induced human carcinogenesis: an oxidative stress perspective.* Mol Biosyst, 2010. **6**(7): p. 1162-72.

82. Deferme, L., et al., *Cell line-specific oxidative stress in cellular toxicity: A toxicogenomics-based comparison between liver and colon cell models.* Toxicol In Vitro, 2015.

83. Deng, G., et al., *Downregulation of ROS-FIG inhibits cell proliferation, colonyformation, cell cycle progression, migration and invasion, while inducing apoptosis in intrahepatic cholangiocarcinoma cells.* Int J Mol Med, 2014. **34**(3): p. 661-8.

84. van der Wijst, M.G., et al., *Targeting Nrf2 in healthy and malignant ovarian epithelial cells: Protection versus promotion.* Mol Oncol, 2015.

85. Takahashi, K., et al., *Purification and characterization of human plasma glutathione peroxidase: a selenoglycoprotein distinct from the known cellular enzyme.* Arch Biochem Biophys, 1987. **256**(2): p. 677-86.

86. Hodges, N.J., et al., *Cellular protection from oxidative DNA damage by over-expression of the novel globin cytoglobin in vitro.* Mutagenesis, 2008. **23**(4): p. 293-8.

87. Thuy le, T.T., et al., *Promotion of liver and lung tumorigenesis in DEN-treated cytoglobin-deficient mice.* Am J Pathol, 2011. **179**(2): p. 1050-60.

88. Geng, R., et al., *Oxidative stress-related genetic polymorphisms are associated with the prognosis of metastatic gastric cancer patients treated with epirubicin, oxaliplatin and 5-Fluorouracil combination chemotherapy.* PLoS One, 2014. **9**(12): p. e116027.

89. Yokoyama, Y., et al., *Protein level of apolipoprotein E increased in human hepatocellular carcinoma.* Int J Oncol, 2006. **28**(3): p. 625-31.

90. Saito, M., M. Kohara, and K. Tsukiyama-Kohara, *Hepatitis C virus promotes expression of the 3beta-hydroxysterol delta24-reductase through Sp1.* J Med Virol, 2012. **84**(5): p. 733-46.

91. Al-Taie, O.H., et al., *Expression profiling and genetic alterations of the selenoproteins GI-GPx and SePP in colorectal carcinogenesis.* Nutr Cancer, 2004. **48**(1): p. 6-14.

92. Calvo, A., et al., *Alterations in gene expression profiles during prostate cancer progression: functional correlations to tumorigenicity and down-regulation of selenoprotein-P in mouse and human tumors.* Cancer Res, 2002. **62**(18): p. 5325-35.

93. Li, C.L., et al., *Selenoprotein P mRNA expression in human hepatic tissues.* World J Gastroenterol, 2007. **13**(16): p. 2363-8.

94. Liang, L., et al., *Dihydroquercetin (DHQ) induced HO-1 and NQO1 expression against oxidative stress through the Nrf2-dependent antioxidant pathway.* J Agric Food Chem, 2013. **61**(11): p. 2755-61.

95. Fan, Y., et al., *The NQO1 C609T polymorphism and hepatocellular carcinoma risk.* Tumour Biol, 2014. **35**(8): p. 7343-50.

96. Ivashkevich, A., et al., *Use of the gamma-H2AX assay to monitor DNA damage and repair in translational cancer research.* Cancer Lett, 2012. **327**(1-2): p. 123-33.

97. Yang, S.F., et al., *Involvement of DNA damage response pathways in hepatocellular carcinoma.* Biomed Res Int, 2014. **2014**: p. 153867.

98. Trachootham, D., J. Alexandre, and P. Huang, *Targeting cancer cells by ROS-mediated mechanisms: a radical therapeutic approach?* Nat Rev Drug Discov, 2009. **8**(7): p. 579-91.

99. Ivanova, D., et al., *The impact of reactive oxygen species on anticancer therapeutic strategies.* Adv Clin Exp Med, 2013. **22**(6): p. 899-908.

100. Tomasetti, M., et al., *Redox-active and redox-silent compounds: synergistic therapeutics in cancer.* Curr Med Chem, 2015. **22**(5): p. 552-68.

101. Fan, C., et al., *Strategy to enhance the therapeutic effect of doxorubicin in human hepatocellular carcinoma by selenocystine, a synergistic agent that regulates the ROS-mediated signaling.* Oncotarget, 2014. **5**(9): p. 2853-63.

102. Sun, W.J., et al., *[The influence of the recombinant lentiviral vectors encoding Hyper-IL-6 on the proliferation of human hepatic cell].* Zhonghua Gan Zang Bing Za Zhi, 2009. **17**(8): p. 615-9.

103. Chebath, J., et al., *Interleukin-6 receptor-interleukin-6 fusion proteins with enhanced interleukin-6 type pleiotropic activities.* Eur Cytokine Netw, 1997. **8**(4): p. 359-65.

104. Peters, M., et al., *Combined interleukin 6 and soluble interleukin 6 receptor accelerates murine liver regeneration.* Gastroenterology, 2000. **119**(6): p. 1663-71.

105. Poussin, K., et al., *Biochemical and functional analyses of gp130 mutants unveil JAK1 as a novel therapeutic target in human inflammatory hepatocellular adenoma.* Oncoimmunology, 2013. **2**(12): p. e27090.

11. Acknowledments

Mein Dank gilt an erster Stelle Herrn Prof. Dr. Ansgar W. Lohse für die Möglichkeit, in seiner Klinik meine Dissertation zu erstellen.

Des Weiteren möchte ich mich bei meinem Doktorvater Herrn PD Dr. med. Henning Wege dafür bedanken, mir ermöglicht zu haben, diese interessante Fragestellung in meiner Doktorarbeit zu bearbeiten und mich stets in herausragender Art und Weise betreut und gefördert zu haben.

Meiner Betreuerin Dr. rer. nat. Denise Heim gilt mein besonderer Dank für die erstklassige Unterstützung in theoretischen und praktischen Fragen zu jedem Zeitpunkt der experimentellen Planung und Durchführung dieser Arbeit.

Auch ohne die exzellente Einarbeitung in wissenschaftliche Methoden durch Martina Fahl und ihre unermüdliche Hilfsbereitschaft wäre die Erstellung meiner Dissertation nicht möglich gewesen.

An dieser Stelle gilt der Dank auch Antonella Carambia, Dorothee Schwinge, Franziska von Haxthausen und Tanja Trautmann, die für eine nette Atmosphäre gesorgt haben und mir die Zeit im Labor deutlich angenehmer gemacht haben.

Por último, quiero dar las gracias a mi familia por su apoyo incondicional. A mi hermano Carlitos por ser el propulsor de mis superaciones profesionales, a mis hermanas Blanca y Pilar por ser el mejor ejemplo que uno puede tener. A mis padres por mi educacion, mis hermanos y su amor que no conocen fronteras. A Marius por creer en mi y compartir conmigo las aventuras de la vida.

This work was supported by a research scholarship from DAAD-La Caixa.

12. Lebenslauf

Mein Lebenslauf wird aus datenschutzrechtlichen Gründen in der elektronischen Version meiner Arbeit nicht veröffentlicht.

13. Eidesstattliche Versicherung

Ich versichere ausdrücklich, dass ich die Arbeit selbständig und ohne fremde Hilfe verfasst, andere als die von mir angegebenen Quellen und Hilfsmittel nicht benutzt und die aus den benutzten Werken wörtlich oder inhaltlich entnommenen Stellen einzeln nach Ausgabe (Auflage und Jahr des Erscheinens), Band und Seite des benutzten Werkes kenntlich gemacht habe.

Ferner versichere ich, dass ich die Dissertation bisher nicht einem Fachvertreter an einer anderen Hochschule zur Überprüfung vorgelegt oder mich anderweitig um Zulassung zur Promotion beworben habe.

Ich erkläre mich einverstanden, dass meine Dissertation vom Dekanat der Medizinischen Fakultät mit einer gängigen Software zur Erkennung von Plagiaten überprüft werden kann.

Unterschrift: ....